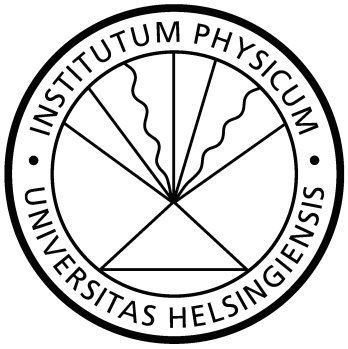

Master's thesis
Meteorology

Contribution of anthropogenic biogenic and non-biogenic emissions to global CH_4 balances by atmospheric inverse modelling

Vilma Eveliina Kangasaho
March 7, 2018

Supervisors: Doc. Tuula Aalto
Dr. Aki Tsuruta
Reviewers: Prof. Timo Vesala
Dr. Maarit Raivonen

UNIVERSITY OF HELSINKI
DEPARTMENT OF PHYSICS

P.O. BOX 64 (Gustaf Hällströmin katu 2)
FIN-00014 University of Helsinki

HELSINGIN YLIOPISTO
HELSINGFORS UNIVERSITET
UNIVERSITY OF HELSINKI
MATEMAATTIS-LUONNONTIETEELLINEN TIEDEKUNTA
MATEMATISK-NATURVETENSKAPLIGA FAKULTETEN
FACULTY OF SCIENCE

Tiedekunta – Fakultet – Faculty	Koulutusohjelma – Utbildningsprogram – Degree programme
Faculty of Science	Degree Programme in Physical Sciences, Meteorology

Tekijä – Författare – Author
Vilma Eveliina Kangasaho

Työn nimi – Arbetets titel – Title
Contribution of anthropogenic biogenic and non-biogenic emissions to global CH_4 balances by atmospheric inverse modelling

Työn laji – Arbetets art – Level	Aika – Datum – Month and year	Sivumäärä – Sidoantal – Number of pages
Master's thesis	7.3.2018	64

Tiivistelmä – Referat – Abstract

The goal of this study is to ascertain whether methane (CH_4) emission can be estimated source-wise by utilising stable isotope observations in the CarbonTracker Data Assimilation System (CTDAS). The global CH_4 budget is poorly known and there are still uncertainties in the spatial and temporal distributions as well as in the magnitude of different sources.

In this study CTDAS- $^{13}CH_4$ atmospheric inverse model is developed. CTDAS-$^{13}CH_4$ is based on ensemble Kalman filer (EnKF) and used to estimate CH_4 fluxes on a region and weekly resolution by implementing CH_4 and $\delta^{13}C$-CH_4 observations. Anthropogenic biogenic emissions (rice cultivation, landfills and waste water treatments and enteric fermentation and manure management) and anthropogenic non-biogenic emissions (coal, residential and oil and gas) are optimised. Different emission sources can be identified by using process-specific isotopic signature values, $\delta^{13}C$-CH_4, because different processes produce CH_4 with different isotopic ratio.

Optimisation of anthropogenic biogenic emissions increased the total emissions from the prior in eastern North America by 34%, while the optimisation of anthropogenic non-biogenic emissions increased only by 14%. In western North America the corresponding changes were -39% and 9%, respectively. In western parts of Europe, total emissions from prior increased in anthropogenic biogenic optimisation by 18% and decreased in non-biogenic by 3%.

Optimisation of anthropogenic biogenic and non-biogenic emissions in the total CH_4 budget did not give complete emission estimates, because the optimisation did not include all emission sources and source-specific $\delta^{13}C$-CH_4 values were assumed not to vary regionally. However, the modelled concentrations from the optimisation of anthropogenic non-biogenic emissions agreed with the observations of CH_4 concentration and $\delta^{13}C$-CH_4 values better. Therefore, one could say that the optimization of anthropogenic non-biogenic emissions was more successful.

This study provides reliable information of the magnitude of anthropogenic biogenic and non-biogenic emissions in regions with sufficient observational coverage. The next step to evaluating the spatial and temporal distributions and magnitude of different CH_4 sources will be optimising all emission sources simultaneously in a multi-year simulation.

Avainsanat – Nyckelord – Keywords
CH_4, $^{13}CH_4$, CTDAS- $^{13}CH_4$, atmospheric inverse modelling, $\delta^{13}C$-CH_4, EnKF

Säilytyspaikka – Förvaringställe – Where deposited
E-thesis (https://ethesis.helsinki.fi)

Muita tietoja – Övriga uppgifter – Additional information

Acknowledgments

I would like express my sincere thanks to my supervisors Doc. Tuula Aalto (FMI: Finnish Meteorological Institute) and Dr. Aki Tsuruta (FMI) for helping and guiding me throughout my work and answering to my questions when needed. Especially, I would like to thank Aki for everything related to CTDAS. I would also like to thank the reviewers of this thesis Prof. Timo Vesala (UH: Uiversity of Helsinki) and Dr. Maarit Raivonen (UH).

Many thanks to Edward Dlugokency (National Oceanic and Atmospheric Administration Earth System Reserach Laboratory) for measuring and analysising CH_4 as well as measuring δ^{13}C-CH_4 observations and thanks to Sylvia Michael (INSTAAR: The Institute of Arctic and Alpine Research) and James White (INSTAAR) for analysing δ^{13}C-CH_4 observations. I also want to acknowledge other WMO GAW data contributiors.

I also want to address thanks to Leif Backman (FMI), Sander Houweling (Netherlands Institute for Space Research), Maarten Krol (WUR: Wageningen University and Research Center), Wouter Peters (WUR), Ingrid van der Laan-Luijkx (WUR), Sebastian Lienert (UB: University of Bern) and Fortunat Joos (UB) for helping with the development of this model.

Without Millennium Youth Camp, I would perhaps not started my studies at the UH. I am thankful to the UH for proving me a good education with many experiences and possibilities. I am grateful that I was offered a summer work at the FMI right after my first year at the university and since that our journey has been continuing. Many thanks for the FMI and especially Carbon Cycle research group for funding my

work. I also want to thank my co-workers at the Carbon Cycle research group for being supportive.

Last but not least, I would also like to thank my family and friends, who has supported me throughout my life and have believed in me whatever I choose to do for my career.

Abbrevations

CTDAS:	Carbon Tracker Data Assimilation System
DEYPTOP:	Dynamical Peatland Model Based on TOPMODEL
EDGAR:	Emission Database for Global Atmospheric Reserach
ECMWF:	European Centre for Medium-Range Weather Forecasts
EnKF:	Ensemble Kalman filter
ERA-Interim:	European Reanalysis climate data
GFED:	Global fire Emission Database
GHG:	Greenhouse Gas
IPCC:	Intergovernmental Panel on Climate Change
MBL:	Marine Boundary Layer
mTC:	Modified TransCom-region
NOAA:	National Oceanic and Atmospheric Administration
NOAA ESRL:	NOAA Earth System Reserach Laboratory
NH:	Northern Hemisphere
PDF:	Probability Density Function
S2:	Optimisation of biogenic emissions
S3:	Optimisation of non-biogenic emissions
SH:	Southern Hemisphere
TC:	TransCom-region
Tg:	Teragram, 10^{12} g

Contents

1 Abstract

The goal of this study is to ascertain whether methane (CH_4) emissions can be estimated source-wise by utilising stable isotope observations in the CarbonTracker Data Assimilation System (CTDAS). The global CH_4 budget is poorly known and there are uncertainties in the spatial and temporal distributions as well as in the magnitude of different sources.

In this study CTDAS-$^{13}CH_4$ atmospheric inverse model is developed. CTDAS-$^{13}CH_4$ is based on ensemble Kalman filer (EnKF) and used to estimate CH_4 fluxes on a region and weekly resolution by implementing CH_4 and δ^{13}C-CH_4 observations. Anthropogenic biogenic emissions (rice cultivation, landfills and waste water treatments and enteric fermentation and manure management) and anthropogenic non-biogenic emissions (coal, residential and oil and gas) are optimised. Different emission sources can be identified by using process-specific isotopic signature values, δ^{13}C-CH_4, because different processes produce CH_4 with different isotopic ratio.

Optimisation of anthropogenic biogenic emissions increased the total emissions from the prior in eastern North America by 34%, while the optimisation of anthropogenic non-biogenic emissions increased only by 14%. In western North America the corresponding changes were -39% and 9%, respectively. In western parts of Europe, total emissions from prior increased in anthropogenic biogenic optimisation by 18% and decreased in non-biogenic by 3%.

Optimisation of anthropogenic biogenic and non-biogenic emissions in the total CH_4 budget did not give complete emission estimates, because the optimisation did not include all emission sources and source-specific δ^{13}C-CH_4 values were assumed

not to vary regionally. However, the modelled concentrations from the optimisation of anthropogenic non-biogenic emissions agreed with the observations of CH_4 concentration and δ^{13}C-CH_4 values better. Therefore, one could say that the optimisation of anthropogenic non-biogenic emissions was more successful.

This study provides reliable information of the magnitude of anthropogenic biogenic and non-biogenic emissions in regions with sufficient observational coverage. The next step in evaluating the spatial and temporal distributions and magnitude of different CH_4 sources will be optimising all emission sources simultaneously in a multi-year simulation.

2 Introduction

The atmospheric burden of methane (CH_4) has more than doubled since pre-industrial times (Hartmann et al., 2013). CH_4 is one of the most potent greenhouse gas (GHG) in the atmosphere and therefore of a high research interest (Saunois et al., 2016b). Evaluating the contributions from anthropogenic non-biogenic (coal, residential and oil and gas) and biogenic (rice cultivation, landfills and waste water treatments and enteric fermentation and manure management) emissions to the global CH_4 budget are crucial in order to better understand of the significance of different sources at both regional and global scales.

Much information on CH_4 emissions sources and sinks is available (Houweling et al., 2017; Kirschke et al., 2013; Mikaloff Fletcher et al., 2004; Tsuruta et al., 2017), but yet the changes in the mean CH_4 concentration in the 21st century remain a mystery (Kirschke et al., 2013). A global model of CH_4 emissions on a source by source basis provides a new insight to the global CH_4 budget (Hein et al., 1997). The

more accurately different emission sources can be evaluated the better the global CH_4 budget components can be understood. To find out the reasons for the changes in the global atmospheric CH_4 concentration, it is useful to look into isotopic ratios together with the total CH_4 concentration and budgets. Hence, CH_4 emission sources can be identified using isotopic signatures, δ^{13}C-CH_4, because different sources produce CH_4 with process-specific isotopic signatures (Mikaloff Fletcher et al., 2004; Monteil et al., 2011).

Inverse models are top-down models and are needed to evaluate atmospheric sources and sinks, because they can compute large amount of data efficiency. Inversion techniques help to reduce the uncertainties in the sources. Inversion methods constrain emission sources using atmospheric transport models by utilising atmospheric measurements of gas concentrations (Houweling et al., 1999).

The first inverse modelling technique for interpreting GHG sources and sinks from atmospheric measurements was introduced by Newsam and Enting (1988). Atmospheric concentration measurements coupled with an atmospheric transport model were used to detect the distribution of carbon dioxide sources and sinks over the surface of the earth. Inversion techniques have developed since then and different types of inversions are used today (Babenhauserheide et al., 2015).

Variational inverse methods require an adjoint model, which is used to calculate the inverse of the observation operator, and the posterior fluxes are obtained by minimising the cost function iteratively with respect to a control matrix (Meirink et al., 2008). On the other hand, variational inverse models can not take advantage of supercomputer power due to sequential algorithms used to minimize the cost function (Houweling et al., 2017). Ensemble Kalman Filter (EnKF), used in this study, is ba-

sed on ensemble filtering method and can efficiently use the supercomputer power. However, ensemble-based methods can not estimate emission to as many regions as variational methods. The ensemble-based methods gained popularity after the power of computers increased (Houweling et al., 2017).

Mathematics behind variational methods and EnKF based inversion models are different but both of them have been proven to produce equally good quality flux estimates. However, computational efficiency is better in EnKF based inversion model and variational is better to resolve temporal correlations (Babenhauserheide et al., 2015).

Various attempts using observations of δ^{13}C-CH_4 have been performed (Bousquet et al., 2011; Mikaloff Fletcher et al., 2004), but the impact to the source distribution estimates has been limited mainly due to limited spatial coverage of the observations, and differences in calibration standards between laboratories (Levin et al., 2012).

This study focuses on inversion-based estimates of global anthropogenic biogenic and non-biogenic CH_4 emissions. CTDAS-CH_4 previously only used CH_4 observations (Tsuruta et al., 2017) but in this study $\delta^{13}CH_4$ was implemented to the CTDAS. In situ measurements of atmospheric CH_4 and δ^{13}C-CH_4 isotopic signature, provided by the NOAA Global Monitoring Division and the Institute of Arctic and Alpine Research (White et al., 2017), are assimilated into the CTDAS-$^{13}CH_4$.

The system uses the TM5 atmospheric transport model (Krol et al., 2005) as an observation operator, converting emissions to concentrations. The model is constrained by ECMWF ERA-Interim meteorological fields (Dee et al., 2011), and uses off-line chemistry fields (Huijnen et al., 2010) to account for the atmospheric CH_4 sinks. ED-

GAR v4.2 FT2010 inventory (EDGAR) is used for prior anthropogenic emissions, LPX-Bern DYPTOP ecosystem model (LPX-Bern, 2016) is used for prior natural CH_4 emissions from wetlands, peatlands and mineral soils and GFED v4 (GFED) is used for prior fire emissions.

The aim of this study is to provide magnitude estimates of anthropogenic non-biogenic and biogenic CH_4 emissions in regions with sufficient observational coverage. This information will help to understand the global CH_4 budget source-wise.

Chapter 3 gives an overview of CH_4 sources and sinks, as well as its C-13 isotope. It also discusses atmospheric transport and annual variation of CH_4 concentrations. Chapter 4 introduces materials and methods used in this study with some clear explanations and examples. In Chapter 5, the results are represented and Chapter 6 gathers the main points of this study.

3 Theory and Background

3.1 CH_4 sources and sinks

CH_4 is emitted from various sources and they can have either natural or anthropogenic origin. Anthropogenic emissions refer to emissions that are caused by human activity, whereas natural emissions are not controlled by humans (Kirschke et al., 2013; Saunois et al., 2016b). The usage of fossil fuels is the largest anthropogenic source (Reddy and DeLaune, 2008), whereas the largest natural source of CH_4 is wetlands. The CH_4 formation processes vary from source to source. In the following Chapters 3.1.1 and 3.1.2, more detailed information about CH_4 emissions from different sources, used in this study, is provided.

3.1.1 Anthropogenic CH_4 sources

Rice cultivation

Rice paddies are an important source of CH_4 and the emission sources are mainly located in tropical Asia (Ciais et al., 2013). Rice is often cultivated in flooded fields, which are favourable for forming methane in oxygen-low conditions in the water-filled soil layers. This is mainly caused by reduction of CO_2 with H_2 (Conrad, 2002). Microbial activity in the soil depends on the soil type, rice variety, temperature and nutrients. Due to the different properties of the soils, CH_4 emissions vary between rice paddies (Conrad, 2002).

Coal

Coalification produces CH_4 and only some of it remains in the coal seam and surrounding rock strata under the pressure. Later, CH_4 is released during the coal mining process chain when the coal is fractured (Irving and Tailkov, 1999). The amount of CH_4 emitted depends on several factors ; coal rank, coal seam depth and mining method are considered to be the most important. Seams have a higher gas content deeper in the ground, and therefore the underground mining releases more CH_4 than the surface mining (Irving and Tailkov, 1999). Coal mining produces more CH_4 than the seams originally contain, because the drop in the pressure releases additional gases from the surrounding strata. Long wall extraction is especially problematic because some of the neighbouring strata is also being fractured (Irving and Tailkov, 1999).

Residential

Residential emissions are only a small source of CH_4. The source contains all fuel combustion in households (Sánchez et al., 2006). Fuels used in the households are, for

example, biomass and fossil fuels, such as coal. CH_4 emissions from the households are mainly due to incomplete burning (Wang et al., 2013).

Oil and Gas

CH_4 emissions from oil and gas consist of all oil and natural gas activities caused by equipment failures, e.g. leaks, evaporation losses, venting, flaring and emissions that are caused by accidents in oil and gas industry (Sánchez et al., 2006). CH_4 emissions from natural gases are an important component of anthropogenic CH_4 emissions and occur mainly due to delivery and end leaks (McKain et al., 2015). Extraction processes of oil also produce CH_4 (Ciais et al., 2013).

Landfills and waste waters treatment

Anaerobic decomposition of organic matter produces CH_4 during wastewater treatment in sewage facilities, from food processing and other industrial facilities. Emissions from landfills and waste water treatments are significant anthropogenic sources of CH_4 (Sánchez et al., 2006).

Enteric fermentation and manure management

Enteric fermentation is a digestive process in which carbohydrates degrade to simple molecules, which are absorbed by the bloodstream. This digestive process in herbivores produces CH_4 as a bi-product. Major sources of CH_4 are ruminant animals, such as, cattle and sheep, whereas non-ruminant animals, such as horses, are only a moderate source. CH_4 is also produced when manure from these animals are decomposed in low-oxygen or anaerobic conditions. In farms manure is stored in large piles or other types of manure management system, such as lagoons, where low-oxygen environment is present (Sánchez et al., 2006).

3.1.2 Natural CH_4 sources

Wetlands

In wetlands (incl. inundated peatland and mineral soils) methanogenic bacteria produces CH_4 by degradation of organic matter in the absence of oxygen. CH_4 produced in wetlands in the water-filled soil layer can escape to the atmosphere by (1) diffusion or (2) direct transport (Reddy and DeLaune, 2008). Direct transport can happen via : (2a) the aerenchyma tissues of plant roots and stems or (2b) ebullition (Reddy and DeLaune, 2008). There are CH_4 emissions from lakes and rivers (Natchimuthu et al., 2017), but they are not included in this study.

Biomass burning

Incomplete burning of biomass produces CH_4 both in smouldering and flaming phases. Forest fires produce CH_4 especially during the smouldering phase whereas grass fires during the flaming phase. This difference is explained by the fact that smouldering phase for forest fires last many hours and the burning is not efficient whereas for grass fires the most biomass burning in the flaming phase and smouldering phase lasts at most only couple of minutes (Hao and Ward, 1993). These emissions can also be considered as anthropogenic emissions as not all forest and grass fires are flamed by nature. Controlled burn of fields in the spring before the start of crop growing season is still a habit, especially in the eastern European countries and Russia. However, separation of those anthropogenic biomass burning emissions from other natural sources is not done in this study.

Termites

Termites have anaerobic bacteria living in their guts, which causes CH_4 production (Sanderson, 1996). The process is the same as for natural wetlands (Ciais et al., 2013).

The dietary type of termites has a strong influence on the emitted CH_4 (Brauman et al., 1992). Termites do not exist northern than temperate region (Wood et al., 1982). The total CH_4 emission from termites to the global CH_4 budget is small (Ciais et al., 2013).

Oceans

Although 70% of Earth is covered by the oceans, CH_4 emitted to the atmosphere from the oceans only contribute approximately 2-3% of the total global CH_4 budget (Ciais et al., 2013). CH_4 from ocean water columns are emitted due to processes such as microbial-mediated diagenesis of sediment organic matter, leaks from near-surface petroleum deposits and decomposition of CH_4 clathrate hydrates (Reeburgh, 2007). In the coastal run-off regions CH_4 emissions are transported to the open ocean water column by diffusion, through seeps and vents. In addition, mud volcanoes may emit fluids containing CH_4 or bubbles with CH_4 (Reeburgh, 2007).

3.1.3 Atmospheric CH_4 sinks

A part of the CH_4 in the atmosphere is removed by atmospheric sinks. The atmospheric removal processes are an important part of the global CH_4 cycle. CH_4 sinks in the atmosphere are located in troposphere and stratosphere. The number of different chemical removal reactions in the stratosphere is larger than in the troposphere. CH_4 has two main sink processes in the stratosphere. The reaction with hydroxyl radical (OH) is important both in troposphere and stratosphere. Reaction with oxygen atom in excited singlet state ($O(^1D)$) is a minor sink in the stratosphere. The largest sink of CH_4 is the reaction with OH (1) in the troposphere (Ciais et al., 2013). Reactions with OH accounts for approximately 90% of the removal processes.

$$CH_4 + OH \rightarrow CH_3 + H_2O \quad (1)$$

$$CH_4 + O(^1D) \rightarrow CH_3 + OH \quad (2)$$

A minor sink of CH_4 in the stratosphere is a reaction with chlorine (Cl). The reaction (3) with Cl has been suggested to happen, but still debated, in the marine boundary layer (Allan et al., 2007).

$$CH_4 + Cl \rightarrow CH_3 + HCl \quad (3)$$

3.1.4 Soil CH_4 sinks

The second largest sink of methane is soils. Some of the CH_4 can be diffused to soils, where oxidation by aerobic bacteria destroys CH_4. Soils are responsible for 6-10% of the total CH_4 removal (Reddy and DeLaune, 2008). The consumption of CH_4 depends on the soil type and availability of soil inorganic nitrogen (Keller et al., 1990).

3.2 Global total CH_4 budget

Currently CH_4 sources are larger than the sinks, which means that the CH_4 is accumulated in the atmosphere and the atmospheric concentration of CH_4 is increasing. If CH_4 emissions would completely be cut down, the atmospheric concentration of CH_4 would first increase a bit due to natural sources and only later on decrease due to the life-time of about 9 years (Ciais et al., 2013).

The CH_4 budget during years 2000-2009 by bottom-up estimates is summarised in Table 1. Troposphere OH is the largest sink of CH_4, being over 80% of the total sink. All other sinks are minor.

TABLE 1 – *Botton-up estimates of global total CH_4 budget during 2000-2009 and their uncertainties. Modified from (Kirschke et al., 2013).*

	$TgCH_4yr^{-1}$
Natural sources	**347 [238-484]**
Natural wetlands	217 [177-284]
Termites	11 [2-22]
Geological (incl. oceans)	54 [33-75]
Others	65 [26-103]
Anthropogenic sources	**331 [304-368]**
Agriculture and waste	200 [187-224]
Biomass burning (incl. biofuels)	35 [32-39]
Fossil fuels	96 [85-105]
Sinks	**632 [492-830]**
Tropospheric OH	528 [454-617]
Stratospheric OH	51 [16-84]
Soils	28 [9-47]
Others	25 [13-37]

3.3 CH_4 isotopes

Isotopes are 'species' of elements, which differ by the number of neutrons in the atomic nucleus but have the same number of protons and electrons (Dawson and Brooks, 2001). CH_4 molecule consists of one carbon and four hydrogen atoms and has carbon or hydrogen isotopes. The stable carbon and hydrogen isotopes are C-12 and C-13, and H-1 and H-2, respectively. C-12 represents 98.9% of the total amount carbon, whereas the natural abundance of C-13 is only around 1.1%. The natural abundance of H-1 is 99.98%, whereas H-2 his 0.02%. Thus, most of the carbon atoms are of type C-12 and most of the hydrogen are of type H-1. In this study, the carbon isotopes are of particular interest, because CH_4 source can be differentiated with the help of this particular isotope.

3.3.1 Isotopic signatures

Isotopic signature expresses the ratio of the stable or unstable isotopes of a particular element in the compound. The difference between atomic masses of the same element affects properties where mass plays a role, such as chemical kinetic behaviour, which leads to natural isotopic separation processes. In this study, only carbon isotopes of CH_4 are taken into account. The C-13 CH_4 isotopic signature, δ^{13}C-CH_4 also called delta values, is expressed as follows

$$\delta^{13}\text{C-CH}_4 = \left(\frac{(^{13}\text{CH}_4/^{12}\text{CH}_4)_{\text{source}}}{\text{R}_{\text{standard}}} - 1\right) \times 1000‰, \tag{4}$$

where $\text{R}_{\text{standard}}$ is standard value for $^{13}\text{CH}_4/^{12}\text{CH}_4$, and $(^{13}\text{CH}_4/^{12}\text{CH}_4)_{\text{source}}$ is the ratio of the heavier isotope to the lighter one in the emission sources. In this study, $\text{R}_{\text{standard}}$ is set to 0.0112372 following Monteil et al. (2011). Each source process has a specific isotopic signature. For fractionating processes, such as kinetic fractionation, that are sensitive to the mass, the isotopic signature value depends if the process prefer lighter or heavier atomic masses. Fractionating processes using more heavier isotopes have a larger δ^{13}C-CH_4 values, whereas processes preferring lighter isotopes have smaller δ^{13}C-CH_4 values. For example the δ^{13}C-CH_4 value for biomass burning depends on the plant photosynthesis pathway. In general, anthropogenic sources are more enriched with the heavier C-13 than biogenic sources, and therefore have higher isotopic signatures. This study assumes the delta values following Monteil et al. (2011) listed in Table 2.

TABLE 2 – *Isotopic signature values for each source used in this study.*

Source	δ^{13}C-CH_4 (‰)
Termites	-57
Oil and Gas	-40
Wetlands	-59
Ocean	-59
Fire	-21.8
Enteric fermentation and Manure management	-62
Landfills and waste water treatment	-55
Rice cultivation	-63
Coal	-35
Residential	-38

3.4 Atmospheric dynamics and transport mechanisms

The main atmospheric transport mechanism is the winds. CH_4 has a lifetime of approximately 9 years (Ciais et al., 2013), which means that it can be easily mixed in the atmosphere. In the vertical direction, the mixing between the troposphere and stratosphere takes approximately 10 years, while within the stratosphere and troposphere it takes only a couple of years. The significant difference in the mixing times is caused by the stratospheric temperature inversion. The temperature inversion makes it harder for the air to be mixed to the stratosphere. The mixing between Poles takes around one year because the Intertropical Convergence Zone (ITZC) is located at the equator. The mixing within the hemispheres takes a couple of months and mixing in the east-west direction takes only about 2 weeks, due to strong westerly winds. (Jacob, 1999)

3.5 Annual cycle of atmospheric CH_4

The seasonal cycle of CH_4 concentration in the atmosphere follows the Northern Hemisphere (NH) emission seasons. Wetlands are mainly responsible for CH_4 emis-

sions' seasonal cycle and therefore, when the NH is experiencing winter, the wetland emissions are small. A NH time series of CH_4 concentration in the atmosphere is a waveform shape as shown in Figure 1. Most of the CH_4 sources are located in the NH and therefore the concentration level in the NH is higher.

On the other hand, the atmospheric CH_4 sinks are smaller during the NH winter than the summer due to coldness and darkness. Therefore, the CH_4 concentration typically increases towards winter and decreases towards summer. As a result, one might observe two pikes in the seasonal cycle in the most northern north boreal zone – one during winter and the other one in late summer when the wetland emissions are high (Aalto et al., 2007).

The seasonal cycle of anthropogenic emissions is poorly known and not much studied. Zazzeri et al. (2017) studied diurnal cycle of methane with isotopic signatures in London and reported higher delta values during the time of the day when demand of anthropogenic fuels were highest - during mornings and evenings. Therefore according to energy statistics (IEA, 2018) one could assume that anthropogenic emissions have a bimodal seasonal cycle with peaks in the summer and winter. The EDGAR v4.3.2 inventory (Janssens-Maenhout et al., 2017) contains seasonal cycles of each emission components for year 2010 suggesting a bimodal seasonal cycle with enteric fermentation being the largest contributor and the emission peak during the summer being greater than during the winter. Globally the largest contribution of anthropogenic seasonal cycle is enteric fermentation (EDGAR) but there is surely differences location-wise. The seasonal cycle of anthropogenic emission in the city center is surely different than that of suburban area or countryside.

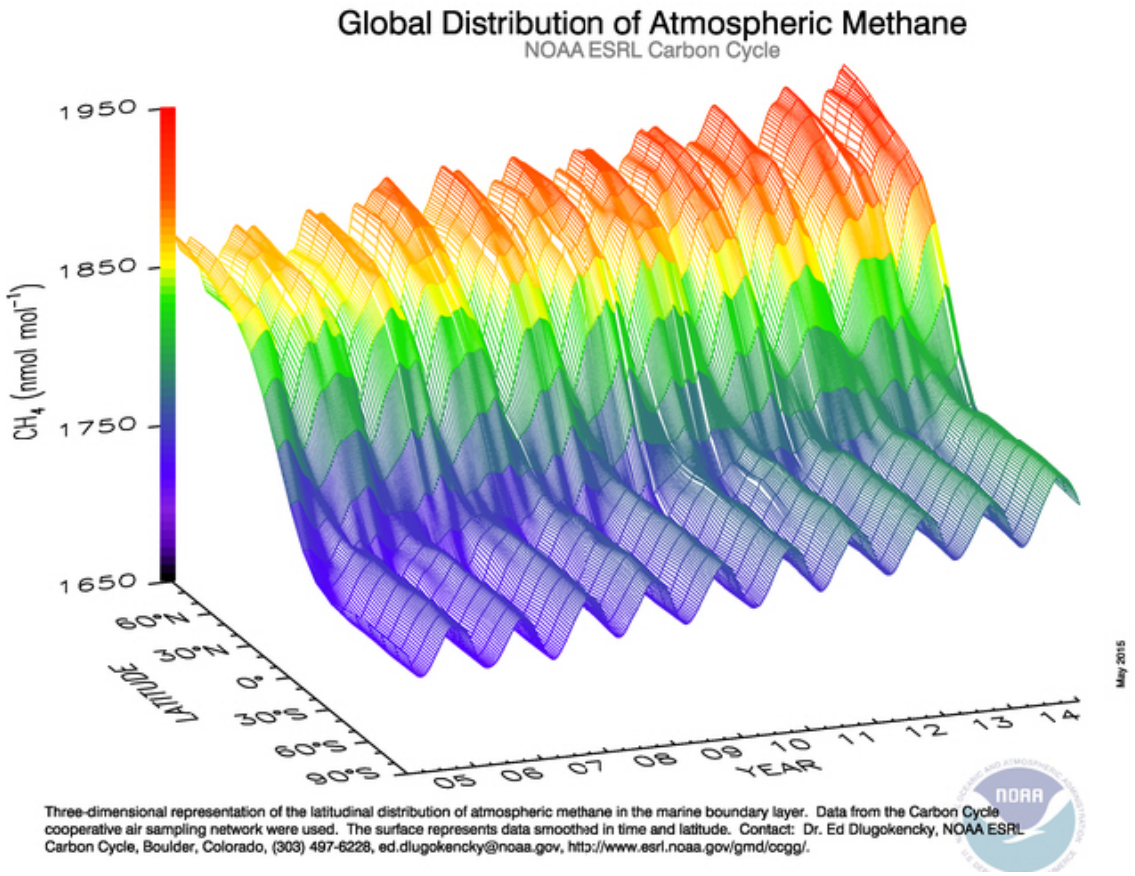

FIGURE 1 – *Latitudinal atmospheric* CH_4 *concentration in marine boundary layer (MBL) as a function of time (NOAA).*

4 Materials and Methods

This study uses several data sources to extend the current knowledge about the topic, and to cover the necessary data inputs for the model runs. The following sections present details of each data source. An overview of the models and data-assimilation procedures will also follow.

4.1 ERA-Interim -data and TM5 transport model

ERA-Interim is a global re-analysis product provided by European Centre for Medium-Range Weather Forecasts (ECMWF). The re-analyses start from 1979 and are continuously updated in real time. ERA-Interim is produced by using a data-assimilation system based on a 2006 release of the IFS (Cy31r2). Analysis window is 12 hours and the system includes a four-dimensional variation analysis. The model uses 60 levels in vertical up to 0.1hPa and has around 80 km horizontal resolution (T255 spectral). The re-analysis product is available for the public and can be freely downloaded from the internet. The product includes several meteorological variables, such as temperature, pressure and wind (Dee et al., 2011). The ERA-Interim data is processed for the TM5 (Krol et al., 2005) resolution and used to constrain the model.

The TM5 is a 3-dimensional (3D) atmospheric chemistry-transport model, which has a 2-way nested zoomed grid with the highest horizontal resolution in $1^\circ \times 1^\circ$. The boundary conditions are updated at every time-step and are consistently taken to the coarsest global model ($6^\circ \times 4^\circ$), to an intermediate resolution of $3^\circ \times 2^\circ$ and to a fine grid of $1^\circ \times 1^\circ$. The number of vertical levels of the TM5 used in this study is 25.

The atmospheric sinks are taken into account in the TM5. Hydroxyl radical (OH) concentration fields are not calculated in the TM5 but are taken from Spivakovsky et al. (2000) and compiled in the TM5 for reactions with CH_4 (Houweling et al., 2014).

4.2 NOAA atmospheric CH_4 and δ^{13}C-CH_4 data

This study uses CH_4 and δ^{13}C-CH_4 measurements from in-situ measurement stations to constrain the the CH_4 emissions in the CarbonTracker Data-assimilation system

(CTDAS). National Oceanic and Atmospheric Administration Earth System Research Laboratory (NOAA ESRL) provides CH_4 measurement data from in-situ stations globally. In addition, the Institute of Arctic and Alpine Research (INSTAAR) provides δ^{13}C-CH_4 measurements globally. The location of the measurement sites, used in the study, are shown on the map in Figure 2. The spatial coverage of the measurement stations is not equally distributed globally. There are regions with no measurements, such as, in the case of δ^{13}C-CH_4, the northernmost Russia. Furthermore, the density of measurement stations in the Southern Hemisphere (SH) is less than in the NH. The observation density is highest in Europe and the USA. Higher observation density enables use of smaller optimisation regions. The measurement data is processed specifically for CTDAS (Tsuruta et al., 2016).

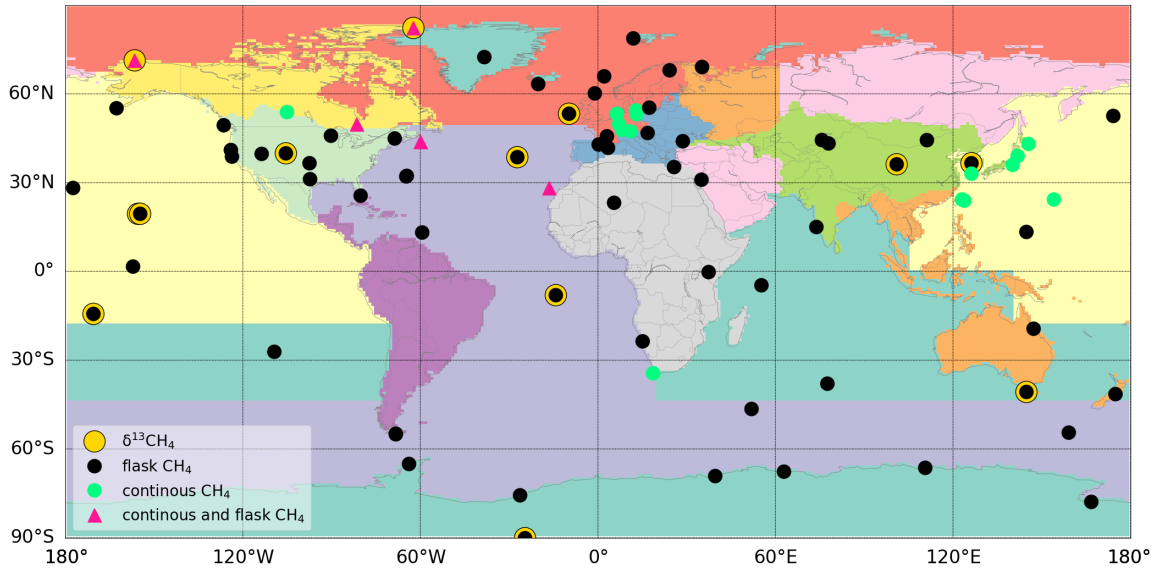

FIGURE 2 – *Location of the measurement sites and type of data used in this study. The golden dots on the map indicates the stations that measure $\delta^{13}C$-CH_4, the black dots indicate the stations with flask measurements of CH_4, the green dots are the stations where CH_4 is measured continuously and the pink triangles are stations that have both continuous and flask measurements of CH_4. Different background colours on the map represent different modified TransCom (mTC)-regions (see Chapter 4.5.3).*

4.3 EDGAR

Emission Database for Global Atmospheric Research (EDGAR ;`http://edgar.jrc.ec.europa.eu/`) provides the budgets of CH_4 from different sources based on IPCC classification in a cooperation with European Commission JRC Joint Research Centre and the Netherlands Environmental Assessment Agency (PBL). EDGAR provides global anthropogenic emissions of GHGs (CH_4, CO_2, N_2O, fluorinated gases) and air pollutants. In this study the CH_4 inventory EDGAR v4.2 FT2010 is used as prior anthropogenic emissions.

Energy balance statistics are used in the direct GHG emission calculations (IEA, 2012). EDGAR uses technology-based emission factor approach in order to calculate emissions for all countries. Emissions (EM) in a country (C) are calculated annually (y) and sector-wise (i) for each compound (x), in this study CH_4, as follows

$$\begin{aligned} EM_{C,i}(y,x) = \sum_{i,j,k} [&AD_{C,i}(y) TECH_{C,i,j}(y) EOP_{C,i,j,k}(y) EF_{C,i,j}(y,x) \\ &(1 - RED_{C,i,j,k}(y,x))], \end{aligned} \tag{5}$$

where AD country-specific activity data quantifying the human activity sector-wise (i), j mix of technologies $TECH$ sector-wise (i), EOP abatement percentage by one of the k end-of-pipe measures for each technology (j), EF country-specific emission factor for each sector (i) and technology (j), and RED relative reduction of uncontrolled emission by installed abatement measure k.

Activity data (AD) was provided by international statistical sources and emission factors (EF) for GHGs were in most cases selected from the 2006 IPCC Guidelines for National Greenhouse Gas Inventories (IEA, 2012). Proxy datasets are used for

gridding the data, and the emissions that are not country specific, such as aviation, are based on spatial allocation of emission sources (Janssens-Maenhout et al., 2013).

Example : CH_4 emissions by biogas production in Finland 2018

The Equation 5 can be applied to calculate the CH_4 emissions (x) from biogas production in Finland in 2018 $EM_{FIN,biogas}(2018, CH_4)$ [kgCH_4/yr]. AD [TJ/yr] in this case would be the consumption of biogas esimated by International Energy Statistics and $TECH$ [%] the share of activity by technology (% of biogas used by factories, energy etc.). EOP [%] is the share of specific abatement measures, which can be for example a catalytic abatement technology for reducing CH_4 emissions in the biogas production. Uncontrolled emission factor is presented by EF [kgCH_4/TJ]. RED [%] is the removal efficiency of abatement measure i.e. the percentage of uncontrolled EF removed. Finally, the Equation 5 in this case becomes

$$\begin{aligned} EM_{FIN,biogas}(2018, CH_4) = \sum_{biogas,j,k} [&AD_{FIN,biogas}(y) TECH_{FIN,biogas,j}(y) \\ &EOP_{FIN,biogas,j,k}(y) EF_{FIN,biogas,j}(2018, CH_4) \\ &(1 - RED_{FIN,CH_4,j,k}(2018, CH_4))]. \end{aligned} \tag{6}$$

Spatial allocation of the country emission is applied to $0.1° \times 0.1°$ resolution. Input to these grids are from a geographical distribution of different activities, such as energy, shipping and agricultural land use. These activities are either point sources or cover larger areas. All these activities are located on a right geographical place using GIS technique. One grid cell can include several countries, and this is solved by multiplying the emission from that grid by the percentage of which that country

occupies in the grid.

EDGAR inventory for annual sector-specific emissions is available from 1970 onwards. The international annual statistics are used as an input to EDGAR. However, this statistic might have a one- to four-year delay. The latest available year is applied for sector- and region-specific monthly profiles to generate global monthly emission maps of $0.1° \times 0.1°$ grid cells.

In this study EDGAR anthropogenic emissions are re-divided into 6 sub-categories (Table 3) following the IPCC source based categorisation (Table 4) and known isotopic signature values : (1) enteric fermentation and manure management, (2) rice cultivation, (3) coal, (4) oil and gas, (5) landfills and waste water, and (6) residential emissions, and the trend of the global total anthropogenic emissions is scaled to match the optimised anthropogenic emissions from CTDAS-CH_4 (Tsuruta et al., 2017). In addition to these categories, emissions from wetlands, termites and oceans are included.

TABLE 3 – *Sectors formed in this study based on EDGAR database.*

Sector	**IPCC class from EDGAR**
Enteric Fermentation and Manure Management	4A, 4B
Landfills and Waste Water Treatment	6A, 6B, 6C
Rice cultivation	4C, 4D
Coal	1B1, 1A1, 1A2
Oil and Gas	1A3a, 1A3c, 1A3d, 1A3e, 1A3b, 1B2a, 1B2b, 2, 7A
Residential	1A4

TABLE 4 – *IPCC CH_4 source division based on 1996 Guidelines (Houghton et al., 1997).*

	IPCC class
Energy	**1**
Fuel Combustion Activities	1A
Energy Industries	1A1
Manufacturing Industries and Construction (ISIC)	1A2
Transport	1A3
Civil Aviation	1A3a
Road Transportation	1A3b
Railways	1A3c
Navigation	1A3d
Other Transportation	1A3e
Other Sectors	1A4
Fugitive Emissions from Fuels	1B
Solid Fuels	1B1
Oil and Natural Gas	1B2
Oil	1B2a
Natural Gas	1B2a
Solvent and Other Product Use	**2**
Agriculture	**4**
Enteric Fermentation	4A
Manure Management	4B
Rice Cultivation	4C
Agricultural Soils	4D
Waste	**6**
Solid Waste and Disposal on Land	6A
Waste Water Handling	6B
Waste Incineration	6C
Other	**7**
Fossil Fuel Fires	7A

4.3.1 Scaling of EDGAR

In this study, the input data form EDGAR-database was scaled to match the known CH_4 budget. The fractions of each component were held constant. The overall trend was decreased because EDGAR suggested higher annual emissions than CTDAS-CH_4, which was taken directly from previous runs (Tsuruta et al., 2017). The annual CH_4 emissions suggested by CTDAS-CH_4 are optimised by using total CH_4 observations rather than the isotope measurements. The scaling was done as follows.

Let F_{orig} be annual total CH_4 flux of one flux component of the grouped EDGAR data (Table 3) for year (yr). The trend (a_{orig}) and intercept (b) were derived from F_{orig}. The fitted mean annual flux (y_{orig}) is

$$y_{orig} = a_{orig} yr + b. \tag{7}$$

Let (ΔF) be the difference between actual data points F_{orig} and fitted data points (y_{orig})

$$\Delta F = F_{orig} - y_{orig}. \tag{8}$$

Knowing the trend of CTDAS-CH_4 data ($CTDAS_{trend}$) and the trend of EDGAR total CH_4 emissions (a_{total}), the new trend (a_{new}) for the EDGAR components was calculated as follows

$$a_{new} = \frac{a_{component} CTDAS_{trend}}{a_{total}}. \tag{9}$$

The new trend corrected annual mean flux is thus

$$F_{new} = a_{new}yr + b + \Delta F. \tag{10}$$

The scaled values of F_{new} are then used as a prior for CTDAS-$^{13}CH_4$ in this study.

4.4 Natural emissions

University of Bern has developed a dynamic global vegetation and land surface process model LPX-Bern (Stocker et al., 2014). The model can describe various processes taking place in the land ecosystems. It can describe dynamical vegetation and terrestrial biogeochemical processes, but it can also integrate representations of non-peatland and peatland ecosystems by taking into account their carbon and nitrogen dynamics. The uptake and release of CO_2, N_2O and CH_4 trace gases is calculated by the model. Vegetation in the LPX-Bern model is represented by various plant functional types, which are competing from the resources in the grid cell. Dynamic coupling of carbon and water cycle through photosynthesis and evapotranspiration is taken into account by the model. LPX-Bern calculates CH_4 emissions and uptake by different ecosystem components such as peatlands, rice paddies and inundated wetlands (LPX-Bern, 2016). In this study, monthly CH_4 fluxes from LPX-Bern are used as prior biospheric emissions.

Global Fire Emission Database (GFED) (Giglio et al., 2013) v4.1 is used because fires are an important source of trace gases, such as CH_4. Satellites that orbit Earth collect much information regarding fire and vegetation activity. GFED combines these to estimate the burned area on a monthly interval. CH_4 emissions can be estimated based on the area information. Currently GFED offers data from 1997 to 2016 with a spatial resolution of 0.25° (GFED).

CH_4 emissions from oceans are calculated using information from sea-water and atmospheric CH_4 mixing ratios. The calculation of CH_4 emissions from oceans is based on the assumption that the ocean surface is supersaturated with respect to CH_4 (Lambert and Schmidt, 1993). Temperature and salinity (Dee et al., 2011) are used to calculate the partial pressure of CH_4 in the water. CH_4 emissions from oceans are calculated from the partial pressure in water and in the atmosphere, which also depend on the wind speed (Tsuruta et al., 2017). This study uses monthly fluxes as a prior. For CH_4 emission from termites an annual mean termite emissions from Ito and Inatomi (2012) are used.

4.5 Flux estimation by inverse modelling

Inverse modelling is a useful tool in estimating fluxes when there is only limited number of observations available in the area of interest. The inversion type used in this study is based on Bayes' theorem. Bayes' theorem starts from the information of spatial distribution and magnitude of fluxes. It uses this information to compute better estimations of fluxes that are consistent with observations. For instance, this study estimates CH_4 fluxes based on atmospheric CH_4 and δ^{13}C-CH_4 observations.

4.5.1 Bayes' theorem

Bayes' theorem is used to calculate probabilities based on a priori information i.e. what is already known before performing the calculation. Let w be a variable or event of interest, q be an observation. The Bayes' theorem states

$$P(w|q) = \frac{P(q|w)P(w)}{P(q)}, \tag{11}$$

where $P(w|q)$ is probability density function (PDF) of w given q, $P(q|w)$ is PDF of y given w, $P(w)$ is PDF of w under all possible outcomes. $P(q)$ is PDF for q under all possible outcomes. In this study $P(q)$ is PDF of the observation q, under all possible outcomes. $P(q|w)$ is the likelihood, telling how probable the observation happens under the hypothesis. $P(w|q)$ is called posterior and it is the best guess for the variable of interest. $P(w)$ is the starting point and also called prior.

4.5.2 Ensemble Kalman filter

Ensemble Kalman filter (EnKF) (Evensen, 2009) is used as a data-assimilation method in this study. EnKF is a recursive filter, which is especially useful in problems with many variables to be estimated (Evensen, 2009). EnKF starts from initial states and calculates prediction values. Then it compares the predicted values to observed ones and tries to push them closer together by considering statistics of both the observations and predicted values. The result of this is the analysed values, that are used to calculate the prediction values in the next time step. EnKF estimate the model uncertainty from samples of an ensemble. The number of ensemble members is hard to choose, because the larger the number of members is the more computationally expensive the simulation will be, but on the other hand, as the number of members increases the accuracy of the result increases (Evensen, 2009).

The new prediction values are calculated as

$$\boldsymbol{\lambda}^{f}_{n,t+1} = \mathcal{M}(\boldsymbol{\lambda}^{a}_{n,t}) + \boldsymbol{\eta}, \tag{12}$$

where $\mathcal{M}$ is a forward model, $\boldsymbol{\eta}$ is the forward model error matrix, $\boldsymbol{\lambda}$ is the ensemble field, and t is the time. A subscript n refers to each ensemble member, f to predicted and a to analysed values. In the first timestep, analysed values are assumed to be the

initial values.

The analysed values are calculated as

$$\boldsymbol{\lambda}^{a}_{n,t} = \boldsymbol{\lambda}^{f}_{n,t} + \mathbf{K}(\mathbf{y}^{\circ}_{t} - \mathcal{H}(\boldsymbol{\lambda}^{f}_{n,t})), \tag{13}$$

where $\mathcal{H}$ is the observation operator, $\mathbf{y}^{\circ}$ the observations and $\mathbf{K}$ the Kalman gain defined as

$$\mathbf{K} = \mathbf{P}\mathbf{H}^{T}(\mathbf{H}\mathbf{P}\mathbf{H}^{T} + \mathbf{R})^{-1}, \tag{14}$$

where $\mathbf{P}$ is the prior error covariance matrix for the ensemble field, $\mathbf{H}$ the linearised observation operator and $\mathbf{R}$ is the observation error covariance matrix.

Prior error covariance matrix is calculated as

$$\boldsymbol{P} = \boldsymbol{\Lambda}\boldsymbol{\Lambda}^{T} = \frac{1}{N-1}\sum_{n=1}^{N}(\boldsymbol{\lambda}^{f}_{n} - \overline{\boldsymbol{\lambda}^{f}})(\boldsymbol{\lambda}^{f}_{n} - \overline{\boldsymbol{\lambda}^{f}})^{T}, \tag{15}$$

where $\overline{\boldsymbol{\lambda}^{f}}$ is the ensemble mean and N the total number of ensemble.

In this study $\mathbf{y}^{\circ}$ are the atmospheric CH_4 and δ^{13}C-CH_4 observations, $\boldsymbol{\lambda}$ is the scaling factors of the CH_4 fluxes. The ensemble field $\boldsymbol{\lambda}$ is generated and $\mathbf{R}$ is constructed based on Tsuruta et al. (2017).

4.5.3 CTDAS-$^{13}CH_4$

CarbonTracker Data Assimilation System-$^{13}CH_4$ (CTDAS-$^{13}CH_4$) is a system that provides information on the global CH_4 distribution. As discussed in previous Chapters (3.1.1 - 3.1.2) CH_4 is emitted from various sources, both from anthropogenic

and natural origins. CTDAS-$^{13}CH_4$ takes contribution of each source into account. It includes different modules for different sources and functionalities (see Figure 3). The modules that are represented in the system are ocean, fossil fuels, agriculture and waste, natural, fire, observations, chemistry, TM5 chemical transport and Ensemble data-assimilation (see Figure 3). For data-assimilation prior fluxes, observations and transport model are needed.

CTDAS-$^{13}CH_4$ uses EnKF as a model scheme, in which TM5 is the observation operator. TM5 is responsible of the chemistry transport and it takes initial 3D concentration files and meteorological data from ECMWF as an input. TM5 also uses prior emission fields to model the new concentration. EnKF is used to optimise scaling factors, which can be further used to calculate the optimised CH_4 fluxes. In the case of CTDAS-$^{13}CH_4$ the EnKF (Chapter 4.5.2) components are listed in the Table 5.

TABLE 5 – *EnKF components for CTDAS-$^{13}CH_4$.*

$\boldsymbol{\lambda}$:	emission scaling factors
$\mathcal{M}$:	forward model
$\mathcal{H}$:	TM5
$\mathbf{y}^\circ$:	atmospheric CH_4 and δ^{13}C-CH_4 observations

TM5 cannot be linearised and therefore Kalman gain (eq. 14) is calculated in parts using approximations for $\mathbf{PH}^T$ and $\mathbf{HPH}^T$ (Peters et al., 2005). Scaling factor field is decomposed to mean state and deviation from the mean state as follows

$$\boldsymbol{\lambda} = \overline{\boldsymbol{\lambda}} + \boldsymbol{\lambda}', \tag{16}$$

where $\overline{\boldsymbol{\lambda}}$ is the mean state and $\boldsymbol{\lambda}'$ the deviation from the mean state. Now the approximations become

$$\mathbf{HPH}^T \approx \frac{1}{N-1}(\mathcal{H}(\boldsymbol{\lambda}'_1), \mathcal{H}(\boldsymbol{\lambda}'_2), ..., \mathcal{H}(\boldsymbol{\lambda}'_N))(\mathcal{H}(\boldsymbol{\lambda}'_1), \mathcal{H}(\boldsymbol{\lambda}'_2), ..., \mathcal{H}(\boldsymbol{\lambda}'_N))^T \quad (17)$$

and

$$\mathbf{PH}^T \approx \frac{1}{N-1}(\mathbf{x}'_1, \mathbf{x}'_2, ..., \mathbf{x}'_N)(\mathcal{H}(\mathbf{x}'_1), \mathcal{H}(\mathbf{x}'_2), ..., \mathcal{H}(\mathbf{x}'_N))^T. \quad (18)$$

CTDAS-$^{13}CH_4$ optimises scaling factors for a certain region (in this study modified TransCom-region, mTC) and time. TC-regions originate from TransCom experiment (`http://transcom.project.asu.edu/`). The posterior flux can then be computed as follows

$$F^{total}(r, z) = \lambda F^{prior\prime}(r, z) + F^{prior}(r, z), \quad (19)$$

where r is a region (mTC-region), z time, $\lambda F^{prior\prime}$ optimised emission and F^{prior} prior emissions.

This study focuses on anthropogenic emissions, and wetland, ocean, fire and termite emissions or atmospheric chemical sinks are not optimised.

Figure 3 shows how CTDAS-$^{13}CH_4$ operates. CTDAS-$^{13}CH_4$ optimises CH_4 fluxes starting from the prior fluxes and resulting in the optimised fluxes. At the very beginning the initial concentration field, meteorological data from ERA-Interim and prior emission fields are used as an input to the TM5 atmospheric transport model. TM5 gives the estimated atmospheric concentrations and together with that, prior emission fields and observed atmospheric concentrations are used as an input to EnKF to obtain optimised emission fields. The optimisation is done for each mTC (see Figure

2) and time step. The optimisation of CH_4 fluxes is done on a weekly basis. In this study the assimilation window length (Peters et al., 2005) was set to be one week, which means that the posterior is calculated only once, and the result is approved immediately.

Process specific δ^{13}C-CH_4 isotopic signatures are assigned to each emission source to estimate $^{13}CH_4$ fractions in CH_4 emissions. Among the priors, anthropogenic non-biogenic and biogenic emissions are optimised and others are directly imposed from the prior (Tsuruta et al., 2017) except natural emissions that are directly taken from LPX-Bern.

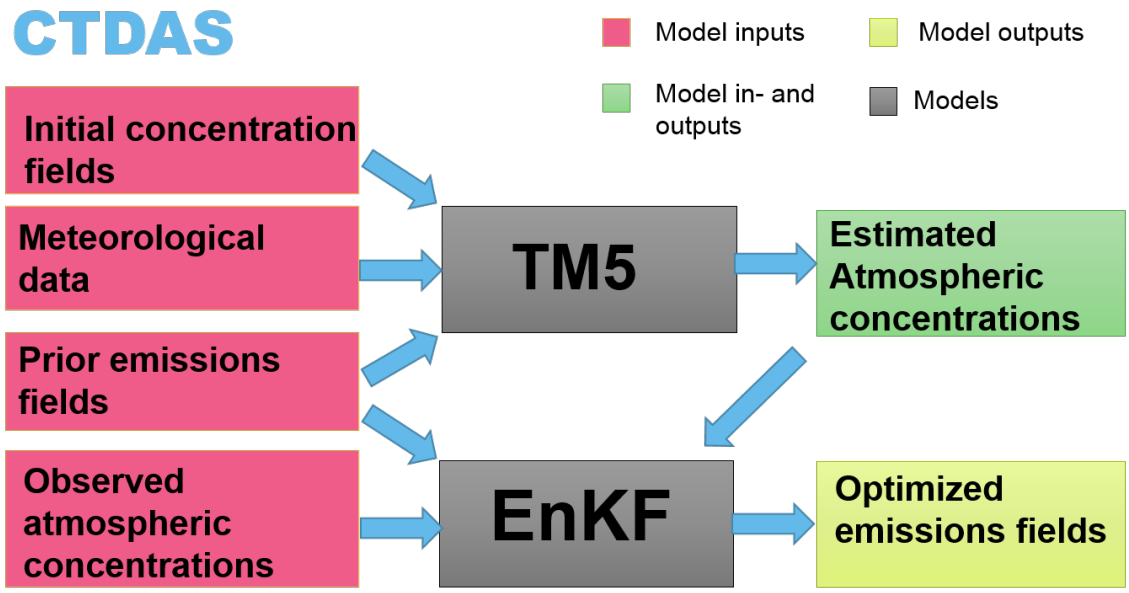

FIGURE 3 – *CTDAS-$^{13}CH_4$ scheme including model input data, atmospheric transport model TM5, EnKF data-assimilation routine and model outputs.*

4.6 Simulation setups

In a spin-up TM5 uses a constant initial concentration field of CH_4 as an input to the model. Constant initial field means that the atmospheric concentration is taken to be constant throughout troposphere and stratosphere. For TM5 to reach the actual CH_4 distribution in the atmosphere, it is required that a realistic meteorological, surface flux and atmospheric chemistry forcing is applied for several times. This is called the spin-up of the model.

Spin-up of the model is really important, because if the unbalanced concentration field is used in estimations of posterior emission fields, it will affect the results. In this study, year 2000 (366 days) was run several times in order to reach a more balanced situation.

In this study, CTDAS-$^{13}CH_4$ was performed twice for years 2000-2003. Different emission sources were optimised in these runs. Run S2 optimised emissions from rice cultivation, landfills and waste water treatments, and enteric fermentation and manure management, whereas run S3 optimised coal, residential and oil and gas. This division was done based on the specific isotopic signatures (see Table 2).

For the first time, when CTDAS is implemented to use δ^{13}C-CH_4-observations, it is better to optimise emissions with similar specific isotopic signatures simultaneously instead of optimising all emissions together due to the large differences in delta values. Optimising all emission simultaneously could potentially lead to failure in constraining different emission sources. In this study, the optimisation was done separately to biogenic (S2) and non-biogenic (S3) emissions. S2 optimises emissions from rice cultivation, enteric fermentation and manure management, whilst S3 optimises coal,

residential, oil and gas. All other emissions, that were not optimized, were taken as priors.

The initial concentration fields of ^{13}C-CH_4 were constructed from previous CTDAS-CH_4 runs by assuming a vertical profile for δ^{13}C-CH_4 values. The mean surface δ^{13}C-CH_4 value was assumed to be $-42‰$, whereas the highest model level was set to $-10‰$ (Röckmann et al., 2011; Saueressig et al., 2001). Distribution of the concentration in latitude, longitude and vertical direction was similar to the initial distribution of CH_4.

5 Results

5.1 TM5 spin-up

The development of the concentration, given constant ^{13}C-CH_4 concentration field (21.5ppb) everywhere, can be seen from the Figure 4. It can be clearly seen that the concentration field is constant in the beginning, and after that it starts to decrease and finally it reaches equilibrium. The lighter spots in the graph indicate the seasonal cycle (see also Figure 5). The average methane concentration during the NH summer is smaller than during the NH winter, because the sink is higher. During wintertime the sink is very small, and the average concentration becomes larger.

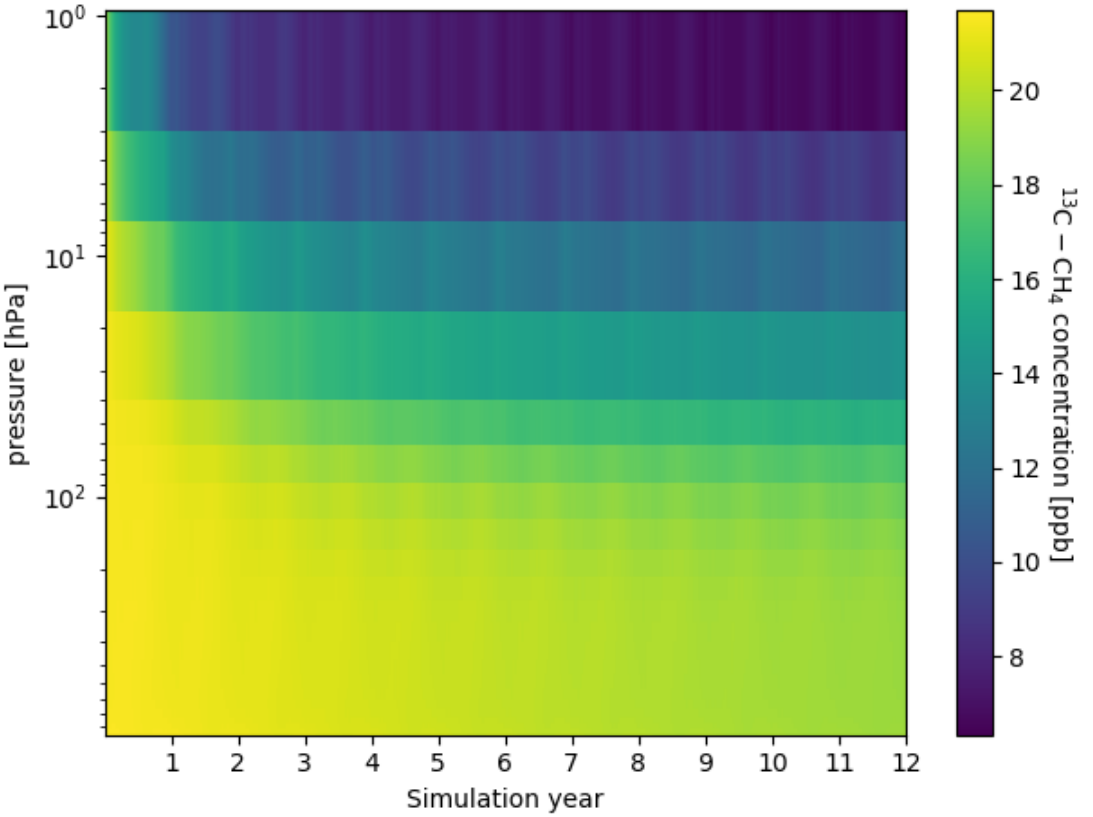

FIGURE 4 – *Atmospheric global mean ^{13}C-CH_4 concentration for 12 years from the spin-up starting from constant emissions field globally and constant concentration in all vertical levels.*

TM5 spin-up of ^{13}C-CH_4 took 8 years in total. The atmosphere reached a steady state during this spin-up period as evidenced by the changes between subsequent years being 10^{-25} ppb. Tsuruta et al. (2017) performed a three-year spin-up of CH_4 in order to receive a well-mixed initial conditions. The spin-up time for TM5 used in this study was longer than in other studies (Huijnen et al., 2010; Tsuruta et al., 2017) because this was the first time to perform ^{13}C-CH_4 spin-up and thus accurate well-mixed conditions throughout the atmosphere were required. However, the result from ^{13}C-CH_4 spin-up was not used in the CTDAS optimisation because matching of

the isotopic signatures values to the observed values was difficult. Instead the initial concentration field was constructed from previous results as described in Chapter 4.6.

Figure 5 shows the two lowest levels of methane concentration as a function of time and pressure. From Figure 5 it can be seen that the highest concentration peaks appear in the NH winter months, while the concentration is at lowest from April to September.

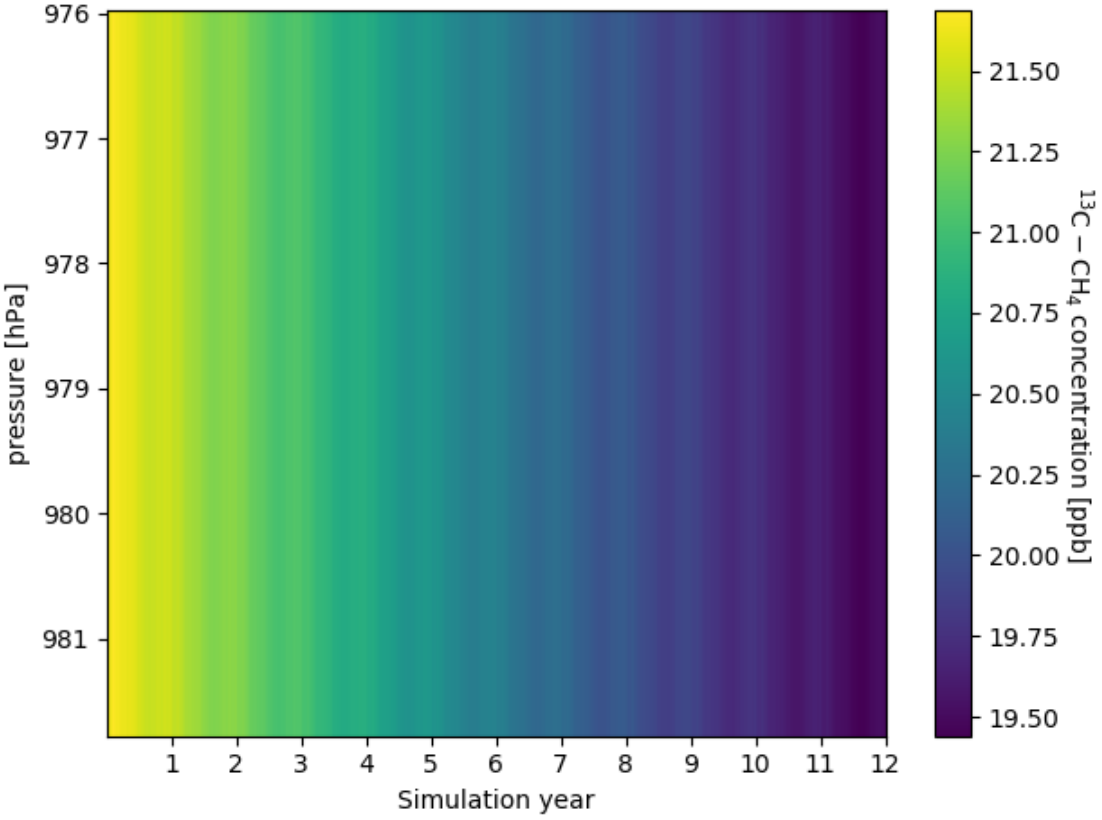

FIGURE 5 – *Atmospheric global mean ^{13}C-CH_4 concentration in the lower atmosphere (up to 2nd TM5 level from the surface) starting from constant emission field globally and constant concentration in all vertical levels.*

5.2 Evaluation of CTDAS-$^{13}CH_4$

Figure 6 shows that the CH_4 concentration is underestimated compared to the observed values with an exception in S3 (non-biogenic) in northern mid-latitudes. Concentrations are computed from ensemble mean modelled concentrations during studied years at the measurement stations. Posterior concentration bias is similar to prior concentration bias in the SH. The bias in the NH in S3 is smaller than in S2 (biogenic). In the NH, the posterior results are better because they do not follow prior intensively. S3 run changed more from the prior, which means the optimisation is working better than in S2.

Bruhwiler et al. (2014) optimised CH_4 emissions without including δ^{13}C-CH_4 observations, and obtained similar biases as in this study. In their study, running optimisation for more years increased the quality of the optimisation. This might indicate that running optimisation including δ^{13}C-CH_4 observations for more years in future, will lead to better estimations.

Monteil et al. (2013) optimised CH_4 emissions without including δ^{13}C-CH_4 observations. Modelled CH_4 concentration were lower than the observed concentrations nearly all time, expect in the northern mid-latitudes. The bias was largest in the SH. However, combining satellite observations with surface observations increased the optimisation quality in the SH and tropics. The differences in their results are due to model set-ups and boundary conditions.

The delta values are underestimated in all latitudes and the bias is largest near the equator (Figure 7). It can also be seen that the model wants to produce larger delta values, which corresponds to the contribution of larger non-biogenic sources or

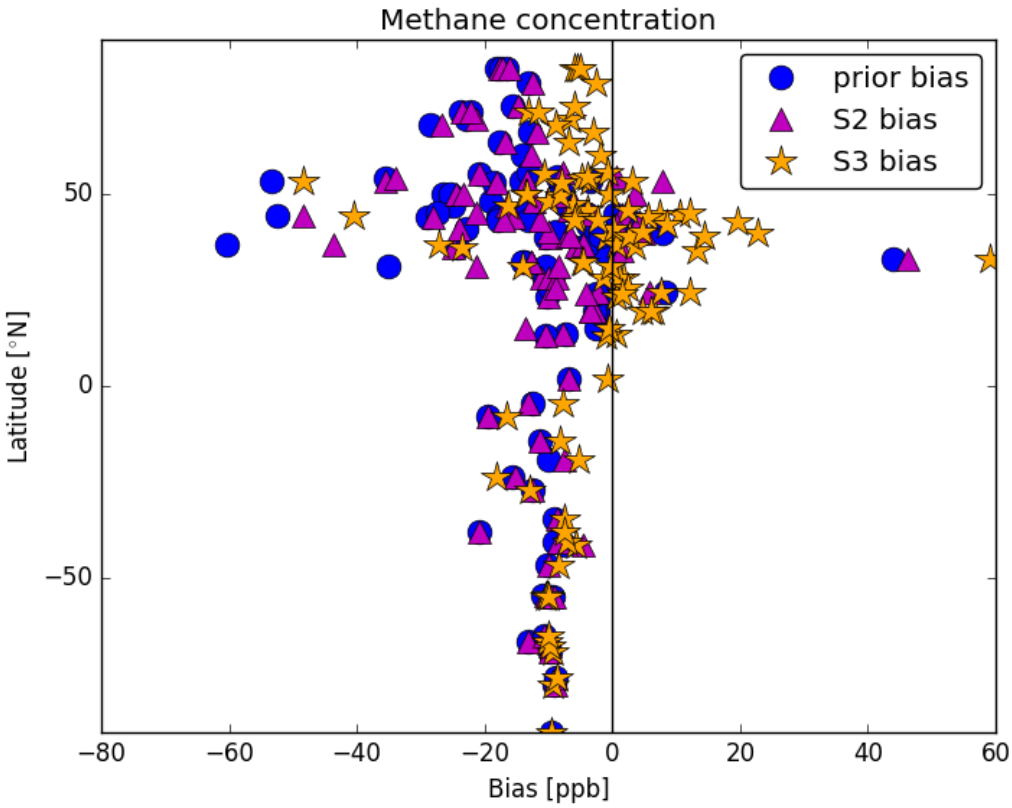

FIGURE 6 – *Methane concentration bias at atmospheric measurement stations as a function of latitude. The bias is calculated by subtracting mean observation value from mean model value. Positive values indicate model overestimation and negative model underestimation, respectively.*

smaller biogenic sources. It seems that S3 has smaller bias than the prior or S2, which indicates that S3 flux estimates are better than the prior or S2.

Monteil et al. (2011) scenario simulation (1970-2010) suggested larger CH_4 concentration and isotopic signatures during 2000-2003 than observations at four measurement stations (Barrow (NH), Mauna-Loa (NH), Cape-Grim (SH) and Arrival Heights (NH)), by using 3-D atmospheric transport model TM3 assuming constant natural sources and growth-rates as in EDGAR4.0 inventory. The best simulation for delta

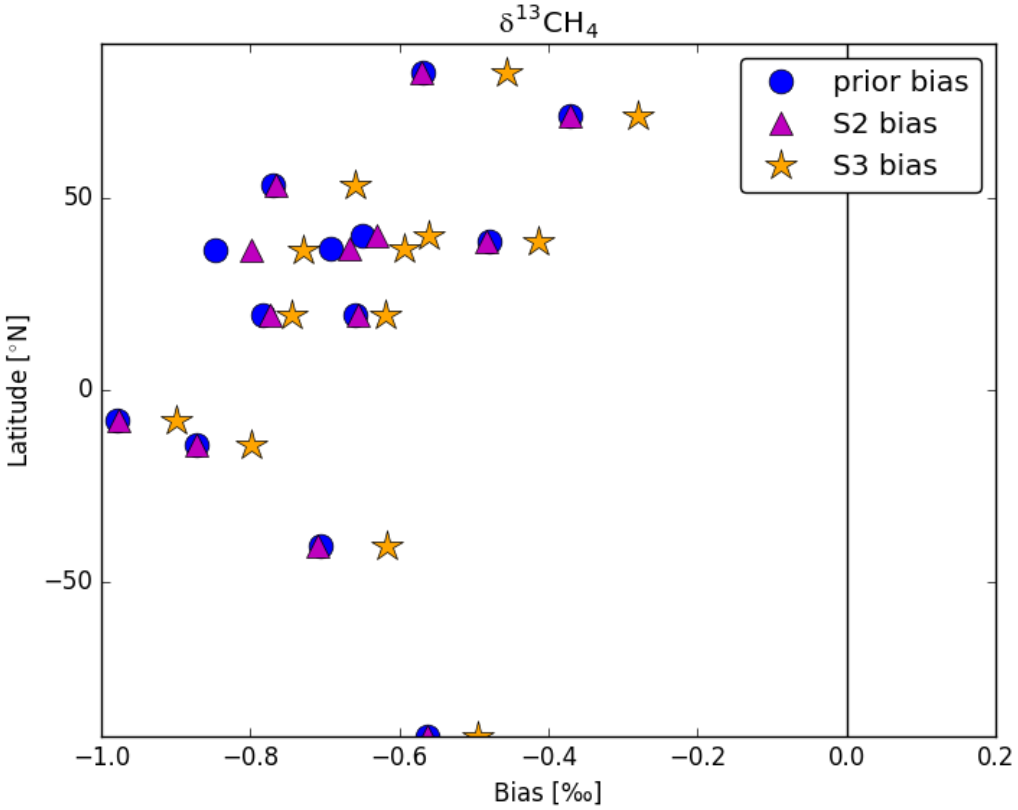

FIGURE 7 – *$\delta^{13}C$-CH_4 bias at atmospheric measurement stations as a function of latitude. Bias is calculated by subtracting mean observation value from mean model value. Positive values indicate model overestimation and negative model underestimation, respectively.*

values was obtained when 1) increasing wetland emissions by 1.5% yr^{-1} after 2000, 2) reducing of biomass burning emissions by 5% in 2000, 10% in 2001 and 2009, 15% between 2002 and 2004 and 20% between 2005 and 2008 or 3) applying fossil fuel growth-rate of 1% yr^{-1} after 2000. However, all simulations with good agreement to measured delta values suggested increased CH_4 emissions after 2000. Monteil et al. (2011) concluded that only one change cannot explain the observed CH_4 or δ^{13}C-CH_4 pattern but high-quality time series of δ^{13}C-CH_4 could provide important additional constrains of emissions. Therefore optimising all emissions simultaneously in a multi-

year run using CTDAS-$^{13}CH_4$, could potentially give valuable information of emission constrains and year by year changes.

5.3 Optimisation of non-biogenic and biogenic emissions

The modelled global total CH_4 budgets ($Tg\,CH_4\,yr^{-1}$) did not agree perfectly but rather well (Table 6). The changes in global total CH_4 budget in S3 was larger than in S2. The total global CH_4 budget stayed similar to prior in S2, but emissions increased in S3. In theory S2 and S3 should produce the same values because the observations constraining these budgets are the same. As this was not the case it is assumed that the difference in S2 and S3 is due to the difference in magnitude and spatial distribution of the various sources, of which a different source subset is selected for optimisation in S2 and S3. However, the modelled global total CH_4 budgets S2 and S3, during years 2000-2004, are in line with the previous estimations of global total CH_4 budgets (Kirschke et al., 2013; Saunois et al., 2016a; Tsuruta et al., 2017). However, the results are not entirely comparable mainly due to different time frame but serve as a guideline.

Prior non-biogenic emissions do not have a seasonal cycle. However, non-biogenic emissions may have a seasonal cycle, which comes up as a result of the optimisation. If the natural emissions are optimised simultaneously, some of the non-biogenic emissions' seasonal cycle may become part of the seasonal cycle of natural emissions.

TABLE 6 – *Global total CH_4 budgets ($Tg\,CH_4\,yr^{-1}$) for priors and posteriors. The values after ± indicates standard deviation.*

Prior S2	**Posterior S2**	**Prior S3**	**Posterior S3**
515.9 ± 11.9	517.1 ± 7.7	516.6 ± 8.1	537.4 ± 4.6

Time series (Figure 8) of the optimised emissions show a seasonal cycle. As the natural emissions are large, have a strong seasonal cycle, and most of the continents are located at the NH, the CH_4 fluxes are at their largest in the late summer of the NH. The smaller episodes, that occur during the NH winter, are the signal from the SH summer and its natural emissions. During the summer time the posterior fluxes are larger than prior (Figure 8). The fluxes in the winter are smaller in S2 than in S3, while during summer flux estimates are larger in S2 than S3.

As can be seen from Figure 8 (see also Table 6), the prior uncertainty is larger than the uncertainty of the optimised, as expected. Prior uncertainty in S2 is 3.19 Tg CH_4 $month^{-1}$ and in S3 2.15 Tg CH_4 $month^{-1}$ respectively. The difference in prior (S2 and S3) uncertainties is due to different optimised sources and their magnitude (Tsuruta et al., 2017). Mean posterior uncertainty in S2 is 2.05 Tg CH_4 $month^{-1}$ and in S3 1.24 Tg CH_4 $month^{-1}$. The uncertainty reduction is larger in S3 (42.4%) compared to S2 (35.7%). The observations constrained emissions more in S3 than in S2. S2 posterior uncertainties are larger during winter than summer. Respective posterior S3 uncertainties do not seem to have a large seasonal variability.

Figures 9a and 9b show that the emissions in the North American eastern region are increased in both S2 and S3, suggesting that the overall emissions need to be increased in the prior in this region. In the western region of North America it is seen that S2 (Figure 9a) decreases emissions and S3 (Figure 9b) increases. This difference indicates that the biogenic emissions are overestimated, or the non-biogenic emissions are too large. The latter one can be explained by the fact, that isotopic ratios of different sources are complicated, and, in this study, they are combined to only few global values. In reality the isotopic signatures may differ in regions and time (Houweling et al., 2006; Levin et al., 2012; Mikaloff Fletcher et al., 2004; Monteil

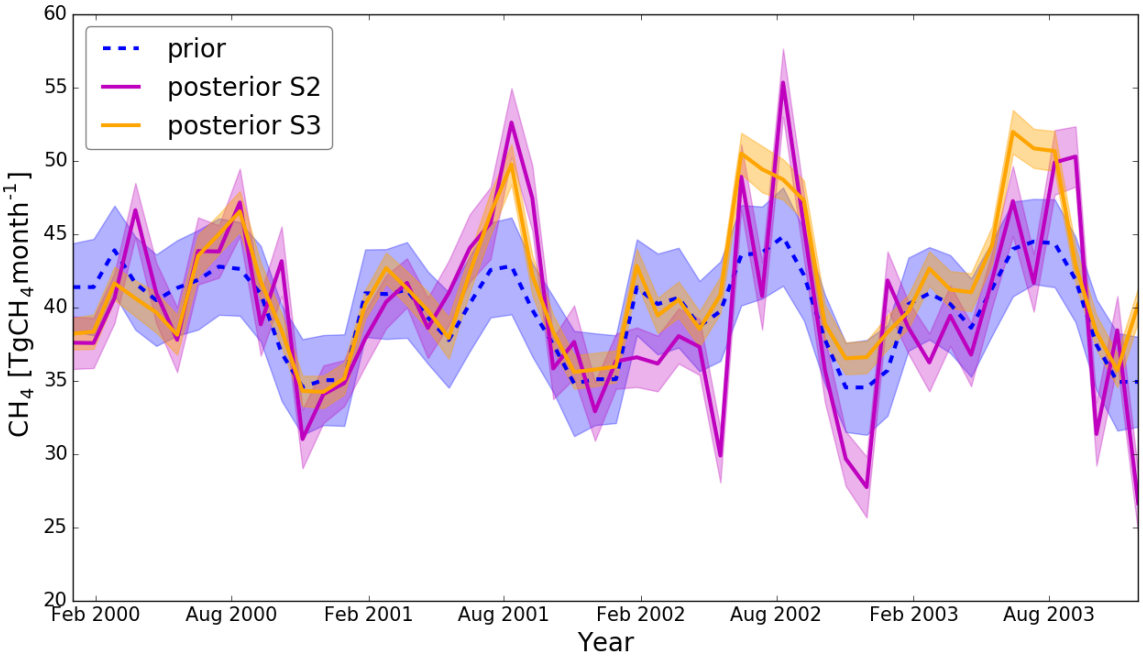

FIGURE 8 – *Time series of monthly mean global total CH_4 budget. The uncertainty range is calculated from the standard deviation of the total emissions from the ensemble. Prior in S2 is shown in the figure.*

et al., 2011). For example Levin et al. (2012) reports delta value for rice to be −65‰ in Vercelli, Italy, while Monteil et al. (2011) uses −62‰ globally. According to Levin et al. (2012) delta values for landfill emissions also vary in depth from −62.9‰ to −52.0‰. If the actual biogenic source has an isotopic signature somewhere between the expected values of biogenic and non-biogenic sources, the model has to increase the modelled isotopic signature to better match the observed values. Both increasing the non-biogenic source and decreasing the biogenic source lead to larger isotopic signatures. In the western Europe, the situation is opposite to that in western North America. This means that either the biogenic emissions are too small or non-biogenic emissions are too large. Mikaloff Fletcher et al. (2004) optimised all emissions including δ^{13}C-CH_4 observations for years 1998-1999 suggesting smaller posterior fluxes in North America and western Europe due to decrease in emission estimates for landfills,

coal in industrial regions and high northern latitude bogs. The optimisation S2 for western North America and S3 for western Europe suggested similar change.

In India, a strong decrease in biogenic emissions is found (Figure 9a). The decrease in the biogenic CH_4 fluxes indicates that the total or biogenic emissions are too large. Non-biogenic emissions in the region are much smaller than the biogenic emissions and therefore, could not be optimised well. Also, in India there is only one measurement flask CH_4 station in the south. Optimisation of non-biogenic and biogenic emission gives different results for the emissions, i.e. S2 suggests that emissions are the same as the priors, while S3 suggests increase from the prior. Emissions in the northern central Russia (Figure 9b) are uncertain because of the lack of observations. In the east coast of China S2 and S3 both decrease emissions in the north (Figure 9a and 9b), while in the south S2 (Figure 9a) shows some increasing signal. According to Mikaloff Fletcher et al. (2004) the decrease is due to the decrease in emissions from rice cultivation and agriculture, whereas the increase due to swamp emission increment. The increase in South America (Figure 9a) is a subject of great uncertainty because S2 suggests an enormous increase compared to S3. This increase might be an artefact and caused by the small number of available observations. Mikaloff Fletcher et al. (2004) suggested the large increase in South America to be primarily driven by the large increase in swamp and biomass burning and secondly by larger estimates of termites and natural gas.

The fluxes cannot be optimised well in regions where only few observations are available (Bruhwiler et al., 2014; Tsuruta et al., 2017). Sometimes the geographical origin of CH_4 emissions is unclear. When there is a forcing need to decrease regional emissions but at the same time a need for increasing global emissions, the global optimisation may lead to a situation where emissions have to be added to regions that

are not well controlled, such as India and South America.

The lack of observations could potentially also lead to dipoles, which however keep the global total budget constant. This means that a dramatic emission decrease appears in some region, whilst a dramatical increase, equally large, occurs somewhere else. The correctness of those dipoles cannot be verified without observations, but if they appear and disappear illogically with respect to changes in spin-up and point in time, are those most likely artefacts.

(a)

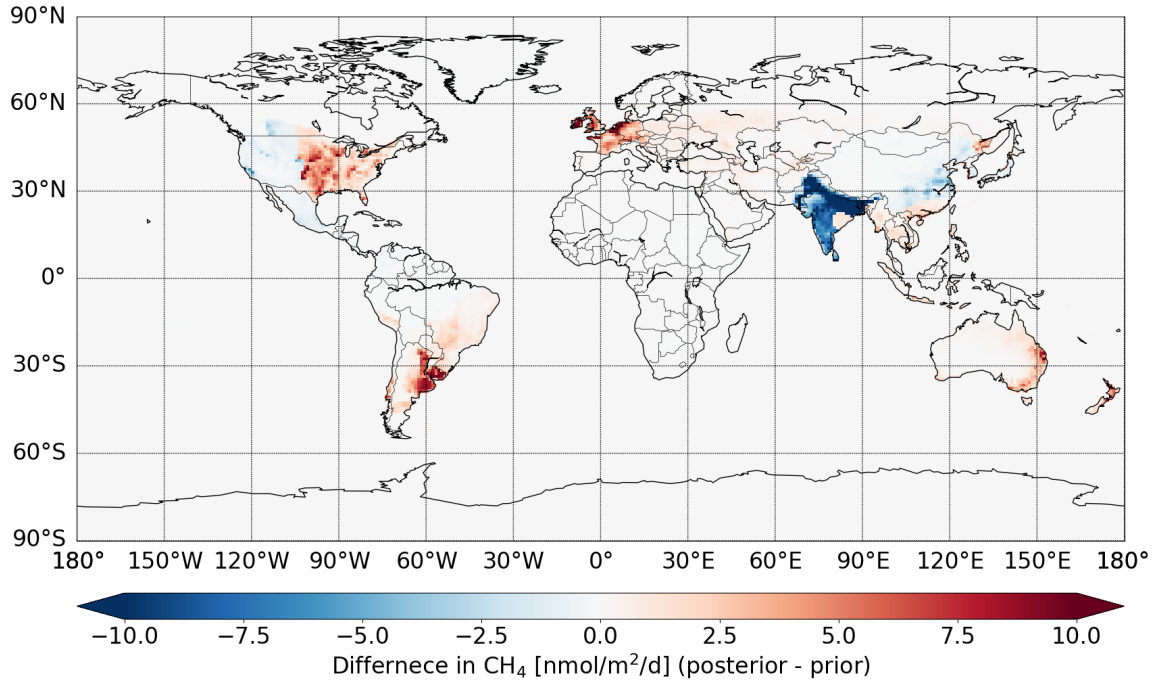

(b)

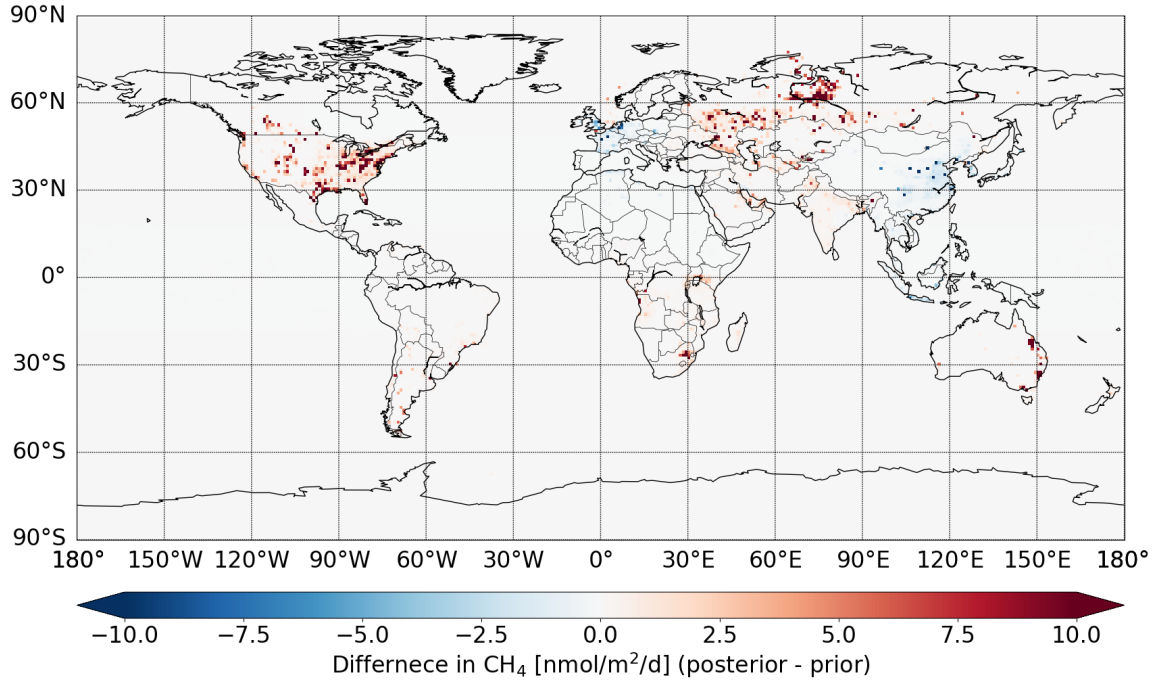

FIGURE 9 – *Total posterior mean minus total prior mean CH_4 emissions for scenarios S2 (a) and S3 (b).*

The percentages of the average relative changes in annual mean total fluxes in the optimisation regions vary a lot (Table 7). Largest changes are in regions where fluxes cannot be constrained well due to the limited availability of data.

Posterior uncertainty in both simulation S2 and S3 decreased in Southeast Asia and eastern North America (Figure 10a and 10b). Optimisation suggested that largest uncertainty reduction happened in S2 in South East China and India, especially near Himalaya (Figure 10a). However, the results can not be verified for regions with only few observations. Uncertainty was also reduced in Northwest Europe, Australian east coast and eastern North America (Figure 10a). In the non-biogenic simulation S3 uncertainty reductions in all regions were equally likely. In contrary to the simulation S2, a reduction in the uncertainty also occurred in Middle East, western North America, Siberia and Ukraine in S3 (Figure 10b).

TABLE 7 – *Average relative change in regional annual mean total fluxes (%).*

Region	**S2**	**S3**
Eastern North America	34	14
Western North America	-39	9
Western Europe	12	-2
South America	14	5
India	-96	7
Northern central Russia	130	177
China	-30	-5
Southeast Asia (inc. southern China)	3.2	-1.2

(a)

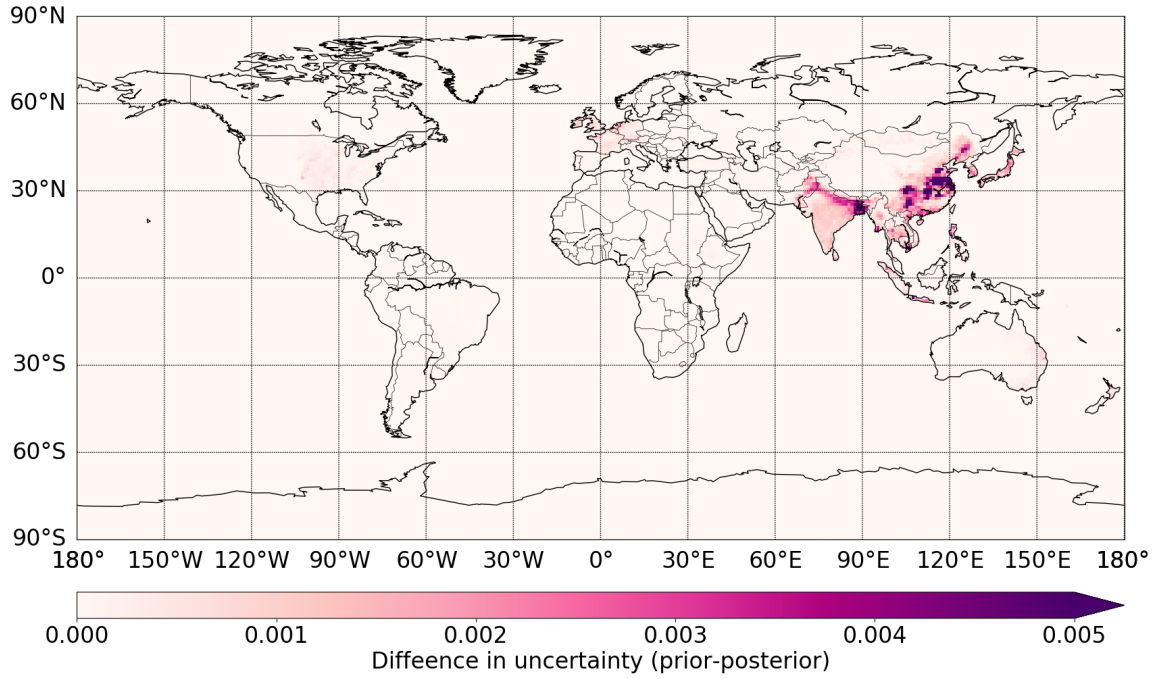

(b)

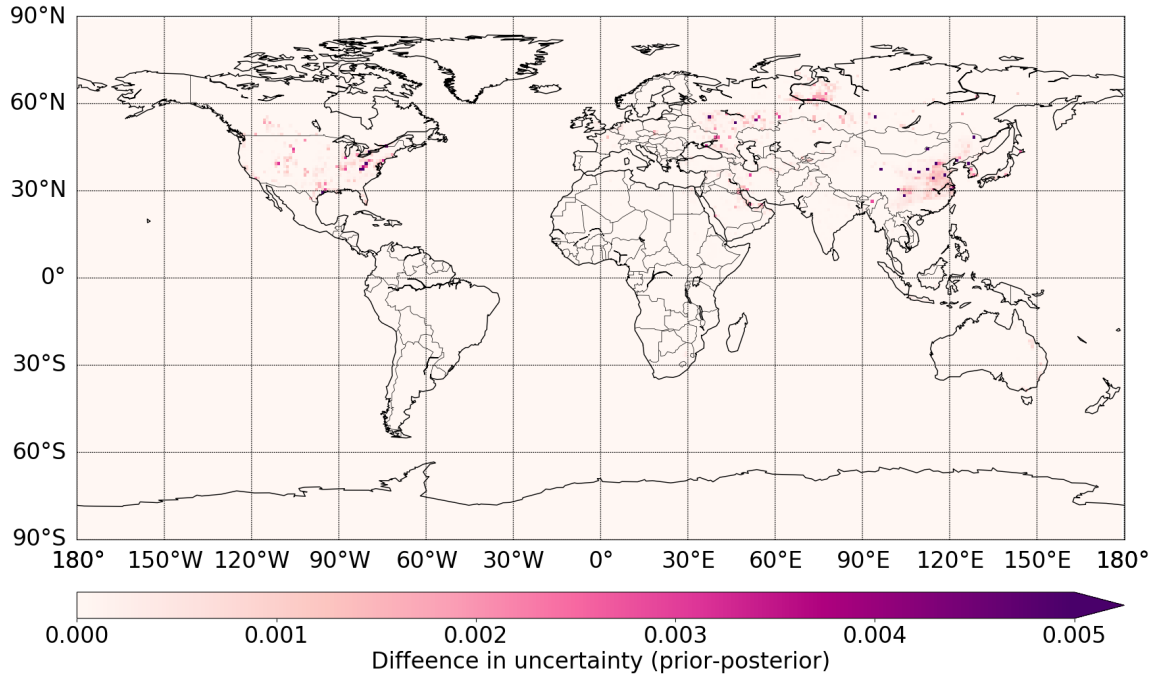

FIGURE 10 – *Prior minus posterior uncertainty for posteriors S2 (a) and S3 (b). The uncertainty is calculated by taking mean of standard deviation in ensemble over time.*

6 Conclusions

In this study CTDAS-$^{13}CH_4$ was developed in order to evaluate the global methane budget source-wise. Spinning up atmospheric transport model TM5 took 8 years. However matching the measured isotopic signatures with modelled signatures in vertical direction was difficult. Therefore initial starting ^{13}C-CH_4 fields were directly computed from previous CH_4 runs with the knowledge of the vertical profile of the isotopic signatures. The CTDAS-$^{13}CH_4$ underestimated atmospheric methane concentrations in all latitudes, expect in the NH mid-latitudes in the S3 optimisation.

S3 optimisation had smaller bias and uncertainty compared to S2. It also changed more from the prior than the S2 optimisation. The total global CH_4 emission estimates were larger than the prior emissions.

The results also showed that problematic areas are near the equator and in the SH. There are not enough observations and the isotopic signatures were underestimated in all optimisations. This might be because one isotopic signature was used for each source globally.

In the future studies, region specific isotopic signatures should be used and the number of observations in the SH and tropics increased. Also, all emission components should be optimised simultaneously. However, optimisation of landfill and waste water treatment emissions might be a bit tricky since they have an isotopic signature between the non-biogenic and biogenic. Fire, oceans and termites are not dominant emission sources and therefore their optimisation is not necessary.

Although optimising non-biogenic and biogenic emissions did not give robust CH_4

emission estimates, the results from inversions are comparable to previous studies (Kirschke et al., 2013; Saunois et al., 2016a; Tsuruta et al., 2017). In the future, when optimising all emission sources together for extended years, the results could potentially give further information about the contribution from different sources to global CH_4 budget.

References

Aalto, T., Hatakka, J., and Lallo, M.: Tropospheric methane in northern Finland: seasonal variations, transport patterns and correlations with other trace gases, Tellus B, 59, 251–259, doi:10.1111/j.1600-0889.2007.00248.x, 2007.

Allan, W., Struthers, H., and Lowe, D. C.: Methane carbon isotope effects caused by atomic chlorine in the marine boundary layer: Global model results compared with Southern Hemisphere measurements, Journal of Geophysical Research: Atmospheres, 112, n/a–n/a, doi:10.1029/2006JD007369, 2007.

Babenhauserheide, A., Basu, S., Houweling, S., Peters, W., and Butz, A.: Comparing the CarbonTracker and TM5-4DVar data assimilation systems for CO_2 surface flux inversions, Atmospheric Chemistry and Physics, 15, 9747–9763, doi:10.5194/acp-15-9747-2015, 2015.

Bousquet, P., Ringeval, B., Pison, I., Dlugokencky, E. J., Brunke, E.-G., Carouge, C., Chevallier, F., Fortems-Cheiney, A., Frankenberg, C., Hauglustaine, D. A., Krummel, P. B., Langenfelds, R. L., Ramonet, M., Schmidt, M., Steele, L. P., Szopa, S., Yver, C., Viovy, N., and Ciais, P.: Source attribution of the changes in atmospheric methane for 2006–2008, Atmospheric Chemistry and Physics, 11, 3689–3700, doi:10.5194/acp-11-3689-2011, 2011.

Brauman, A., Kane, M., D., Labat, M., and Breznak, J., A.: Genesis of Acetate and Methane by Gut Bacteria of Nutritionally Diverse Termites, Science, 257, 1384–1387, doi:10.1126/science.257.5075.1384, 1992.

Bruhwiler, L., Dlugokencky, E., Masarie, K., Ishizawa, M., Andrews, A., Miller, J., Sweeney, C., Tans, P., and Worthy, D.: CarbonTracker-CH_4: an assimilation

system for estimating emissions of atmospheric methane, Atmospheric Chemistry and Physics, 14, 8269–8293, doi:10.5194/acp-14-8269-2014, 2014.

Ciais, P., Sabine, C., Bala, G., Bopp, L., Brovkin, V., Canadell, J., Chhabra, A., DeFries, R., Galloway, J., Heimann, M., Jones, C., Le Quéré, C., Myneni, R., Piao, S., and Thornton, P.: Carbon and Other Biogeochemical Cycles, book section 6, p. 465–570, Cambridge University Press, Cambridge, United Kingdom and New York, NY, USA, doi:10.1017/CBO9781107415324.015, 2013.

Conrad, R.: Control of microbial methane production in wetland rice fields, Nutrient Cycling in Agroecosystems, 64, 59–69, doi:10.1023/A:1021178713988, 2002.

Dawson, T. E. and Brooks, P. D.: Fundamentals of Stable Isotope Chemistry and Measurement, Springer Netherlands, Dordrecht, doi:10.1007/978-94-015-9841-5_1, 2001.

Dee, D. P., Uppala, S. M., Simmons, A. J., Berrisford, P., Poli, P., Kobayashi, S., Andrae, U., Balmaseda, M. A., Balsamo, G., Bauer, P., Bechtold, P., Beljaars, A. C. M., van de Berg, L., Bidlot, J., Bormann, N., Delsol, C., Dragani, R., Fuentes, M., Geer, A. J., Haimberger, L., Healy, S. B., Hersbach, H., Hólm, E. V., Isaksen, L., Kållberg, P., Köhler, M., Matricardi, M., McNally, A. P., Monge-Sanz, B. M., Morcrette, J.-J., Park, B.-K., Peubey, C., de Rosnay, P., Tavolato, C., Thépaut, J.-N., and Vitart, F.: The ERA-Interim reanalysis: configuration and performance of the data assimilation system, Quarterly Journal of the Royal Meteorological Society, 137, 553–597, doi:10.1002/qj.828, 2011.

EDGAR: URL `http://edgar.jrc.ec.europa.eu`.

Evensen, G.: Data Assimilation, Springer Berlin Heidelberg, doi:10.1007/978-3-642-03711-5, 2009.

GFED: URL http://www.globalfiredata.org/index.html.

Giglio, L., Randerson, J. T., and van der Werf, G. R.: Analysis of daily, monthly, and annual burned area using the fourth-generation global fire emissions database (GFED4), Journal of Geophysical Research: Biogeosciences, 118, 317–328, doi: 10.1002/jgrg.20042, 2013.

Hao, W. M. and Ward, D., E.: Methane production from global biomass burning, Journal of Geophysical Research: Atmospheres, 98, 20 657–20 661, doi:10.1029/ 93JD01908, 1993.

Hartmann, D., Klein Tank, A., Rusticucci, M., Alexander, L., Brönnimann, S., Charabi, Y., Dentener, F., Dlugokencky, E., Easterling, D., Kaplan, A., Soden, B., Thorne, P., Wild, M., and Zhai, P.: Observations: Atmosphere and Surface, book section 2, p. 159–254, Cambridge University Press, Cambridge, United Kingdom and New York, NY, USA, doi:10.1017/CBO9781107415324.008, 2013.

Hein, R., Crutzen, P., J., and Heimann, M.: An inverse modeling approach to investigate the global atmospheric methane cycle, Global Biogeochemical Cycles, 11, 43–76, doi:10.1029/96GB03043, 1997.

Houghton, J. T., Meira Filho, L. G., Lim, K., Trennton, I., Mamaty, I., Bonduki, Y., Griggs, D. J., and Callander, B. A.: Revised 1996 IPCC Guidelines for National Greenhouse Gas Inventories, 1 - 3, 1997.

Houweling, S., Kaminski, T., Dentener, F., Lelieveld, J., and Heimann, M.: Inverse modeling of methane sources and sinks using the adjoint of a global transport model, Journal of Geophysical Research: Atmospheres, 104, 26 137–26 160, doi: 10.1029/1999JD900428, 1999.

Houweling, S., Röckmann, T., Aben, I., Keppler, F., Krol, M., Meirink, J. F., Dlugokencky, E. J., and Frankenberg, C.: Atmospheric constraints on global emissions of methane from plants, Geophysical Research Letters, 33, n/a–n/a, doi: 10.1029/2006GL026162, 2006.

Houweling, S., Krol, M., Bergamaschi, P., Frankenberg, C., Dlugokencky, E. J., Morino, I., Notholt, J., Sherlock, V., Wunch, D., Beck, V., Gerbig, C., Chen, H., Kort, E. A., Röckmann, T., and Aben, I.: A multi-year methane inversion using SCIAMACHY, accounting for systematic errors using TCCON measurements, Atmospheric Chemistry and Physics, 14, 3991–4012, doi:10.5194/acp-14-3991-2014, 2014.

Houweling, S., Bergamaschi, P., Chevallier, F., Heimann, M., Kaminski, T., Krol, M., Michalak, A. M., and Patra, P.: Global inverse modeling of CH_4 sources and sinks: an overview of methods, Atmospheric Chemistry and Physics, 17, 235–256, doi:10.5194/acp-17-235-2017, 2017.

Huijnen, V., Williams, J., van Weele, M., van Noije, T., Krol, M., Dentener, F., Segers, A., Houweling, S., Peters, W., de Laat, J., Boersma, F., Bergamaschi, P., van Velthoven, P., Le Sager, P., Eskes, H., Alkemade, F., Scheele, R., Nédélec, P., and Pätz, H.-W.: The global chemistry transport model TM5: description and evaluation of the tropospheric chemistry version 3.0, Geoscientific Model Development, 3, 445–473, doi:10.5194/gmd-3-445-2010, 2010.

IEA: CO2 Emissions from Fuel Combustion 2012, doi:http://dx.doi.org/10.1787/co2_fuel-2012-en, 2012.

IEA: Monthly electricity statistics with data up to November 2017 (http://www.iea.org/statistics/topics/Electricity/), 2018.

Irving, W. and Tailkov, O.: Good Practice Guidance and Uncertainty Management in National Greenhouse Gas Inventories, IPCC, 1999.

Ito, A. and Inatomi, M.: Use of a process-based model for assessing the methane budgets of global terrestrial ecosystems and evaluation of uncertainty, Biogeosciences, 9, 759–773, doi:10.5194/bg-9-759-2012, 2012.

Jacob, D., J.: Introduction to Atmospheric Chemistry, Princeton University Press, 1999.

Janssens-Maenhout, G., Pagliari, V., Guizzardi, D., and Muntean, M.: Global emission inventories in the Emission Database for Global Atmospheric Research (EDGAR) - Manual (I): Gridding: EDGAR emissions distribution on global gridmaps, Publications Office of the European Union, doi:10.2788/81454, 2013.

Janssens-Maenhout, G., Crippa, M., Guizzardi, D., Muntean, M., Schaaf, E., Dentener, F., Bergamaschi, P., Pagliari, V., Olivier, J. G. J., Peters, J. A. H. W., van Aardenne, J. A., Monni, S., Doering, U., and Petrescu, A. M. R.: EDGAR v4.3.2 Global Atlas of the three major Greenhouse Gas Emissions for the period 1970–2012, Earth System Science Data Discussions, 2017, 1–55, doi: 10.5194/essd-2017-79, 2017.

Keller, M., Mitre, M., E., and Stallard, R., F.: Consumption of atmospheric methane in soils of central Panama: Effects of agricultural development, Global Biogeochemical Cycles, 4, 21–27, doi:10.1029/GB004i001p00021, 1990.

Kirschke, S., Bousquet, P., Ciais, P., Saunois, M., Canadell, J., G., Dlugokencky, E., J., Bergamaschi, P., Bergmann, D., Blake, D., R., Bruhwiler, L., Cameron-Smith, P., Castaldi, S., Chevallier, F., Feng, L., Fraser, A., Heimann, M., Hodson, E., L., Houweling, S., Josse, B., Fraser, P., J., Krummel, P., B., Lamarque, J.-F.,

Langenfelds, R., L., Corinne, L., Q., Naik, V., O'Doherty, S., Palmer, P., I., Pison, I., Plummer, D., Poulter, B., Prinn, R., G., Rigby, M., Ringeval, B., Santini, M., Schmidt, M., Shindell, D., T., Simpson, I., J., Spahni, R., Steele, L., P., Strode, S., A., Sudo, K., Szopa, S., Van Der Werf, G., R., Voulgarakis, A., Van Weele, M., Weiss, R., F., Williams, J., E., and Zeng, G.: Three decades of global methane sources and sinks, Nature Geoscience, 6, 813–823, doi:10.1038/ngeo1955, 2013.

Krol, M., Houweling, S., Bregman, B., van den Broek, M., Segers, A., van Velthoven, P., Peters, W., Dentener, F., and Bergamaschi, P.: The two-way nested global chemistry-transport zoom model TM5: algorithm and applications, Atmospheric Chemistry and Physics, 5, 417–432, doi:10.5194/acp-5-417-2005, 2005.

Lambert, G. and Schmidt, S.: Reevaluation of the oceanic flux of methane: Uncertainties and long term variations, Chemosphere, 26, 579 – 589, doi:https://doi.org/10.1016/0045-6535(93)90443-9, 1993.

Levin, I., Veidt, C., Vaughn, B., H., Brailsford, G., Bromley, T., Heinz, R., Lowe, D., Miller, J., B., Poß, C., and White, J.: No inter-hemispheric d13CH4 trend observed, Nature, 486, E3–E4, 2012.

LPX-Bern: Simulating oxygen isotope ratios in tree ring cellulose using a dynamic global vegetation model, data set available at www.climate.unibe.ch, Jul 2016, 2016.

McKain, K., Down, A., Raciti, S., M., Budney, J., Hutyra, L., R., Floerchinger, C., Herndon, S., C., Nehrkorn, T., Zahniser, M., S., Jackson, R., B., Phillips, N., and Wofsy, S., C.: Methane emissions from natural gas infrastructure and use in the urban region of Boston, Massachusetts, Proceedings of the National Academy of Sciences, 112, 1941–1946, doi:10.1073/pnas.1416261112, 2015.

Meirink, J. F., Bergamaschi, P., and Krol, M. C.: Four-dimensional variational data

assimilation for inverse modelling of atmospheric methane emissions: method and comparison with synthesis inversion, Atmospheric Chemistry and Physics, 8, 6341–6353, doi:10.5194/acp-8-6341-2008, 2008.

Mikaloff Fletcher, S., E., Tans, P., P., Bruhwiler, L., M., Miller, J., B., and Heimann, M.: CH4 sources estimated from atmospheric observations of CH4 and its 13C/12C isotopic ratios: 1. Inverse modeling of source processes, Global Biogeochemical Cycles, 18, doi:10.1029/2004GB002223, 2004.

Monteil, G., Houweling, S., Dlugockenky, E., J., Maenhout, G., Vaughn, B., H., White, J., and Rockmann, T.: Interpreting methane variations in the past two decades using measurements of CH_4 mixing ratio and isotopic composition, Atmospheric Chemistry and Physics, 11, 9141–9153, doi:10.5194/acp-11-9141-2011, 2011.

Monteil, G., Houweling, S., Butz, A., Guerlet, S., Schepers, D., Hasekamp, O., Frankenberg, C., Scheepmaker, R., Aben, I., and Röckmann, T.: Comparison of CH4 inversions based on 15 months of GOSAT and SCIAMACHY observations, Journal of Geophysical Research: Atmospheres, 118, 11,807–11,823, doi:10.1002/2013JD019760, 2013.

Natchimuthu, S., Wallin, M. B., Klemedtsson, L., and Bastviken, D.: Spatio-temporal patterns of stream methane and carbon dioxide emissions in a hemiboreal catchment in Southwest Sweden, Scientific reports, 7, 39 729, doi:10.1038/srep39729, 2017.

Newsam, G. N. and Enting, I. G.: Inverse problems in atmospheric constituent studies. I. Determination of surface sources under a diffusive transport approximation, Inverse Problems, 4, 1037, 1988.

NOAA: URL https://www.esrl.noaa.gov/gmd/ccgg/gallery/figures/index.html.

Peters, W., Miller, J. B., Whitaker, J., Denning, A. S., Hirsch, A., Krol, M. C., Zupanski, D., Bruhwiler, L., and Tans, P. P.: An ensemble data assimilation system to estimate CO2 surface fluxes from atmospheric trace gas observations, Journal of Geophysical Research: Atmospheres, 110, n/a–n/a, doi:10.1029/2005JD006157, 2005.

Reddy, K. R. and DeLaune, R. D.: Biogeochemistry of Wetlands: Science and application, CRC Press, 2008.

Reeburgh, W., S.: Oceanic Methane Biogeochemistry, Chemical Reviews, 107, 486–513, doi:10.1021/cr050362v, 2007.

Röckmann, T., Brass, M., Borchers, R., and Engel, A.: The isotopic composition of methane in the stratosphere: high-altitude balloon sample measurements, Atmospheric Chemistry and Physics, 11, 13 287–13 304, doi:10.5194/acp-11-13287-2011, 2011.

Sanderson, M. G.: Biomass of termites and their emissions of methane and carbon dioxide: A global database, Global Biogeochemical Cycles, 10, 543–557, doi:10.1029/96GB01893, 1996.

Saueressig, G., Crowley, J., N., Bergamaschi, P., Brühl, C., Brenninkmeijer, C., and Fischer, H.: Carbon 13 and D kinetic isotope effects in the reactions of CH4 with O(1D) and OH: New laboratory measurements and their implications for the isotopic composition of stratospheric methane, Journal of Geophysical Research: Atmospheres, 106, 23 127–23 138, doi:10.1029/2000JD000120, 2001.

Saunois, M., Bousquet, P., Poulter, B., Peregon, A., Ciais, P., Canadell, J. G., Dlugokencky, E. J., Etiope, G., Bastviken, D., Houweling, S., Janssens-Maenhout, G., Tubiello, F. N., Castaldi, S., Jackson, R. B., Alexe, M., Arora, V. K., Beerling, D. J., Bergamaschi, P., Blake, D. R., Brailsford, G., Brovkin, V., Bruhwiler, L., Crevoisier, C., Crill, P., Covey, K., Curry, C., Frankenberg, C., Gedney, N., Höglund-Isaksson, L., Ishizawa, M., Ito, A., Joos, F., Kim, H.-S., Kleinen, T., Krummel, P., Lamarque, J.-F., Langenfelds, R., Locatelli, R., Machida, T., Maksyutov, S., McDonald, K. C., Marshall, J., Melton, J. R., Morino, I., Naik, V., O'Doherty, S., Parmentier, F.-J. W., Patra, P. K., Peng, C., Peng, S., Peters, G. P., Pison, I., Prigent, C., Prinn, R., Ramonet, M., Riley, W. J., Saito, M., Santini, M., Schroeder, R., Simpson, I. J., Spahni, R., Steele, P., Takizawa, A., Thornton, B. F., Tian, H., Tohjima, Y., Viovy, N., Voulgarakis, A., van Weele, M., van der Werf, G. R., Weiss, R., Wiedinmyer, C., Wilton, D. J., Wiltshire, A., Worthy, D., Wunch, D., Xu, X., Yoshida, Y., Zhang, B., Zhang, Z., and Zhu, Q.: The global methane budget 2000–2012, Earth System Science Data, 8, 697–751, doi:10.5194/essd-8-697-2016, 2016a.

Saunois, M., Jackson, R. B., Bousquet, P., Poulter, B., and Canadell, J. G.: The growing role of methane in anthropogenic climate change, Environmental Research Letters, 11, 120 207, 2016b.

Spivakovsky, C. M., Logan, J. A., Montzka, S. A., Balkanski, Y. J., Foreman-Fowler, M., Jones, D. B. A., Horowitz, L. W., Fusco, A. C., Brenninkmeijer, C. A. M., Prather, M. J., Wofsy, S. C., and McElroy, M. B.: Three-dimensional climatological distribution of tropospheric OH: Update and evaluation, Journal of Geophysical Research: Atmospheres, 105, 8931–8980, doi:10.1029/1999JD901006, 2000.

Stocker, B. D., Spahni, R., and Joos, F.: DYPTOP: a cost-efficient TOPMODEL

implementation to simulate sub-grid spatio-temporal dynamics of global wetlands and peatlands, Geoscientific Model Development, 7, 3089–3110, doi:10.5194/gmd-7-3089-2014, 2014.

Sánchez, M. J. S., Bhattacharya, S., and Mareckova, K.: Reporting Guidance and Tables, vol. 1, IPCC, Prepared by the National Greenhouse Gas Inventories Programme, IGES, Japan, 2006.

Tsuruta, A., Aalto, T., Backman, L., Hakkarainen, J.and van der Laan-Luijkx, I., Krol, M., Spahni, R., Houweling, S., Laine, M., van der Schoot, M., Langenfelds, R., Ellul, R., and Peters, W.: Development of CarbonTracker Europe-CH4 – Part 1: system set-up and sensitivity analyses, pp. 1–31, 2016.

Tsuruta, A., Aalto, T., Backman, L., Hakkarainen, J., van der Laan-Luijkx, I. T., Krol, M. C., Spahni, R., Houweling, S., Laine, M., Dlugokencky, E., Gomez-Pelaez, A. J., van der Schoot, M., Langenfelds, R., Ellul, R., Arduini, J., Apadula, F., Gerbig, C., Feist, D. G., Kivi, R., Yoshida, Y., and Peters, W.: Global methane emission estimates for 2000–2012 from CarbonTracker Europe-CH_4 v1.0, Geoscientific Model Development, 10, 1261–1289, doi:10.5194/gmd-10-1261-2017, 2017.

Wang, Q., Geng, C., Lu, S., Chen, W., and Shao, M.: Emission factors of gaseous carbonaceous species from residential combustion of coal and crop residue briquettes, Frontiers of Environmental Science & Engineering, 7, 66–76, doi:10.1007/s11783-012-0428-5, 2013.

White, J., W. C., Vaughn, B., H., and Michel, S., E.: Stable Isotopic Composition of Atmospheric Methane (13C) from the NOAA ESRL Carbon Cycle Cooperative Global Air Sampling Network, 1998-2015, Version: 2017-01-20, URL `ftp://aftp.cmdl.noaa.gov/data/trace_gases/ch4c13/flask/`, 2017.

Wood, T. G., Johnson, R. A., Bacchus, S., Shittu, M. O., and Anderson, J. M.: Abundance and Distribution of Termites (Isoptera) in a Riparian Forest in the Southern Guinea Savanna Vegetation Zone of Nigeria, Biotropica, 14, 25–39, 1982.

Zazzeri, G., Lowry, D., Fisher, R. E., France, J. L., Lanoisellé, M., Grimmond, C. S. B., and Nisbet, E. G.: Evaluating methane inventories by isotopic analysis in the London region, Scientific Reports, 7, 4854, doi:10.1038/s41598-017-04802-6, 2017.